[American Journal of Science, Vol. 319, October, 2019, P. 694-735, DOI 10.2475/08.2019.03]

PROVENANCE OF THE NEWFOUNDLAND APPALACHIAN FORELAND BASINS

SHAWNA E. WHITE*,†, JOHN W.F. WALDRON*, GREG R. DUNNING**, and S. ANDREW DUFRANE*

ABSTRACT. The tectonic history of the Appalachian orogen is recorded in the adjacent foreland. Offshore seismic data suggest that an initial, Middle Ordovician foreland basin was filled by sources in Newfoundland, whereas the Late Ordovician foreland basin was loaded and filled by sources to the SW, in the Québec segment of the orogen, where NW-vergent Taconian arc-continent collision may have continued later than in Newfoundland. We test this hypothesis using U/Pb ages of detrital zircon within foreland basin successions in western Newfoundland. Previously published results from the oldest foreland succession, the Middle Ordovician Goose Tickle Group, demonstrate ages similar to units preserved with the Humber Arm Allochthon, emplaced during Middle Ordovician Taconic orogenesis, including a predominant Paleoproterozoic peak at 1.85 Ga. In this study we investigated U/Pb geochronology of detrital zircon from younger foreland successions from Upper Ordovician to Devonian. The largest proportion of analyses within all foreland successions fall between 0.95 and 1.3 Ga, with largest peaks occurring between 1.0 and 1.1 Ga, typical of zircon derived from the Grenville Orogen. Earlier Mesoproterozoic and Paleoproterozoic ages range from 1.3 to 2.0. The abundance of Mesoproterozoic grains and conspicuous lack of 1.85 Ga Paleoproterozoic zircon in the overlying Upper Ordovician Long Point Group and latest Silurian to Early Devonian Clam Bank Formation indicates that these sediments were not derived from units within the Humber Arm Allochthon. Probability density plots of continental margin units in the Québec/New England segment of the orogen demonstrate a similar strong Mesoproterozoic and weak Paleoproterozoic signature, suggesting derivation of the Long Point Group from the Québec segment of the orogen. Within the mid-Paleozoic Clam Bank - Red Island Road succession, typical Gondwanan ages are absent and 1.0 Ga grains derived from the Grenville Orogen are abundant. This is consistent with underthrusting of the Gondwanan microcontinents Ganderia and Avalonia during Salinic and Acadian orogenesis. Only Mesoproterozoic zircon grains were found in the Early Devonian Red Island Road Formation, consistent with derivation from Mesoproterozoic Grenville massifs in western Newfoundland or Cape Breton Island which were exhumed during Devonian Acadian inversion.

Key words: Appalachians, Newfoundland, provenance, detrital zircon, foreland basin

INTRODUCTION

Foreland basins provide valuable records of the building of orogens, because they are formed mainly by orogenic loading through flexure of the lithosphere, while the developing orogen provides the source of detritus to fill the basin. The provenance of foreland basin fills provides evidence of exhumation of source regions within the orogen because of this intrinsic link between orogen and basin.

The current understanding of Appalachian orogenesis is based largely on the interpretation of geological datasets (that is, structural, stratigraphic, geochemical and isotopic) collected from deformed, metamorphosed, and magmatic units within the orogen. In Newfoundland, the earliest convergent episode, the Ordovician Taconic Orogeny, involved the collision of an island arc and peri-Laurentian microcontinents

* Department of Earth and Atmospheric Sciences, University of Alberta, Edmonton, Alberta, Canada
** Department of Earth Sciences, Memorial University, St. John's, Newfoundland, Canada
† Corresponding author: swhite4@laurentian.ca

with Laurentia, and westward emplacement of allochthons (including the Humber Arm Allochthon in Newfoundland) on top of the Laurentian margin (Stevens, 1970; Williams and Stevens, 1974; Waldron and van Staal, 2001; van Staal and others, 2009; for a contrary view, see Karabinos and others, 2017). In southern New England, the peri-Gondwanan Moretown Terrane was also emplaced at this time (Macdonald and others, 2014). Later orogenic episodes, including the Silurian Salinic Orogeny (Dunning and others, 1990) and Early Devonian Acadian Orogeny (van Staal and others, 2014) also involved the accretion of exotic terranes to the composite margin. Although stratigraphic and isotopic evidence within the orogen (van Staal and others, 1998; van Staal and others, 2009; Waldron and others, 2019) provides constraint on what accreted and when, many questions remain unanswered. These include: (1) what was the specific location of accreted material prior to Carboniferous reshuffling of terranes along the length of the orogen; (2) which portions of the orogen were exhumed and contributed detritus to the developing basin; and (3) what was the variability in load position and magnitude along the orogen during orogenesis? In particular, recently published work (White and others, 2019) has suggested that a Late Ordovician foreland-basin succession (the Long Point Group) located offshore of western Newfoundland was the result of loading in the Québec portion of the orogen, to the southwest. We aim to test this hypothesis by comparing the provenance of the Long Point Group and overlying foreland-basin strata with potential sources in the northern Appalachians.

We present analyses of five samples from the foreland basin successions in western Newfoundland (fig. 1). The foreland sediments were largely derived from erosion of thrust sheets of allochthonous continental margin and local basement units (Bradley, 1983; Cawood and Nemchin, 2001; McLennan and others, 2001; Thomas and Becker, 2007). We discuss our new data in comparison with previously published zircon ages from the Paleozoic continental margin and regional basement and aim to provide new interpretations of Appalachian orogenic history in context of the current tectonic understanding of the orogen.

TECTONIC SETTING AND SOURCE REGIONS

Laurentian Basement

The Appalachian Orogen developed on the Paleozoic continental margin of eastern Laurentia, itself founded on Mesoproterozoic and older basement rocks (fig. 2) (Cawood and Nemchin, 2001). The Superior and North Atlantic cratons, that represent the Archean cores of eastern Laurentia, were stitched together by 2.0 to 1.8 Ga Paleoproterozoic orogens (Hoffman, 1988). In eastern Laurentia these include: the Trans-Hudson, New Québec, Torngat, and Makkovik orogens. Along the eastern margin of Laurentia lies the Grenville Province (Rivers, 1997) dominated by the ~ 1.0 Ga Grenville Orogen, although older pre-Grenvillian crust (1.7–1.2 Ga) is also preserved within the Grenville Province (Rivers, 1997) (fig. 2). Populations of zircon sourced from Laurentia generate age spectra with characteristic peaks and gaps indicative of derivation from these provinces; a number of studies show excellent examples of such Laurentia-derived zircon (figs. 3R and 3S) and the associated probability density distributions which characterize eastern Laurentian sources (Cawood and Nemchin, 2001; Cawood and others, 2007b; Waldron and others, 2008; Waldron and others, 2012). The probability density function shown in figure 3R is a typical Laurentian signature with major peaks at 1.1, 1.8 and 2.7 Ga coinciding with the ages of major Laurentian crustal components.

The western zone of the Appalachian Orogen, the Humber Zone (fig. 1), contains deformed Paleozoic rocks of Laurentian affinity and older Mesoproterozoic basement of the Grenville Province (Rivers, 1997; Heaman and others, 2002). In Newfoundland,

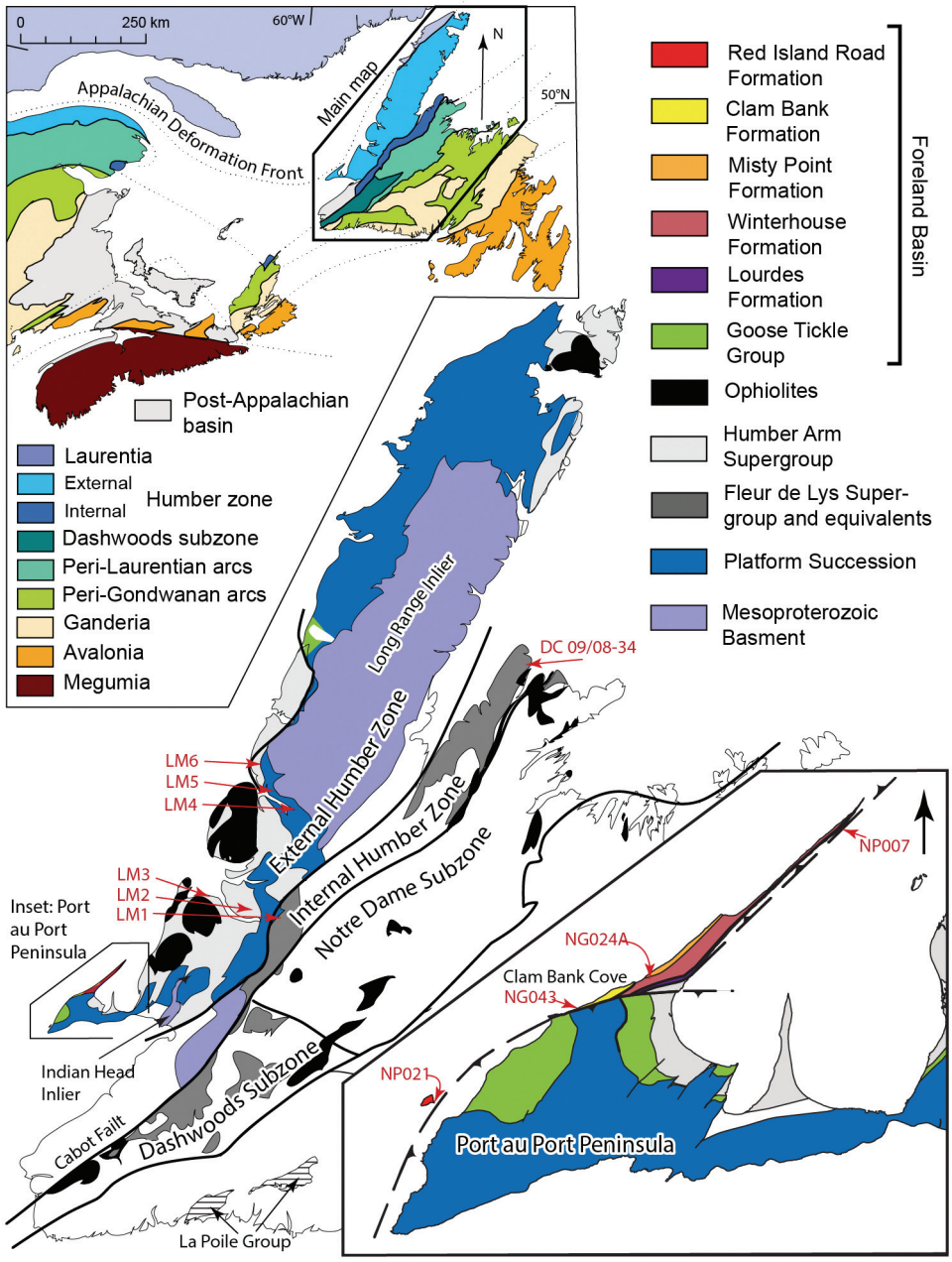

Fig. 1. Geological map of western Newfoundland showing place names, locations, structures, and sample sites from previously published works. Inset A is a tectonic zonation map of a portion of the northern Appalachians (modified from Waldron and van Staal, 2001). Inset B is a geological map of the Port au Port Peninsula showing sample sites from this study.

it is divided into a western, external subzone, in which Paleozoic strata are largely unmetamorphosed, and an eastern, internal zone of mainly metamorphic rocks. To the east, the Notre Dame subzone is interpreted by most authors as built on the

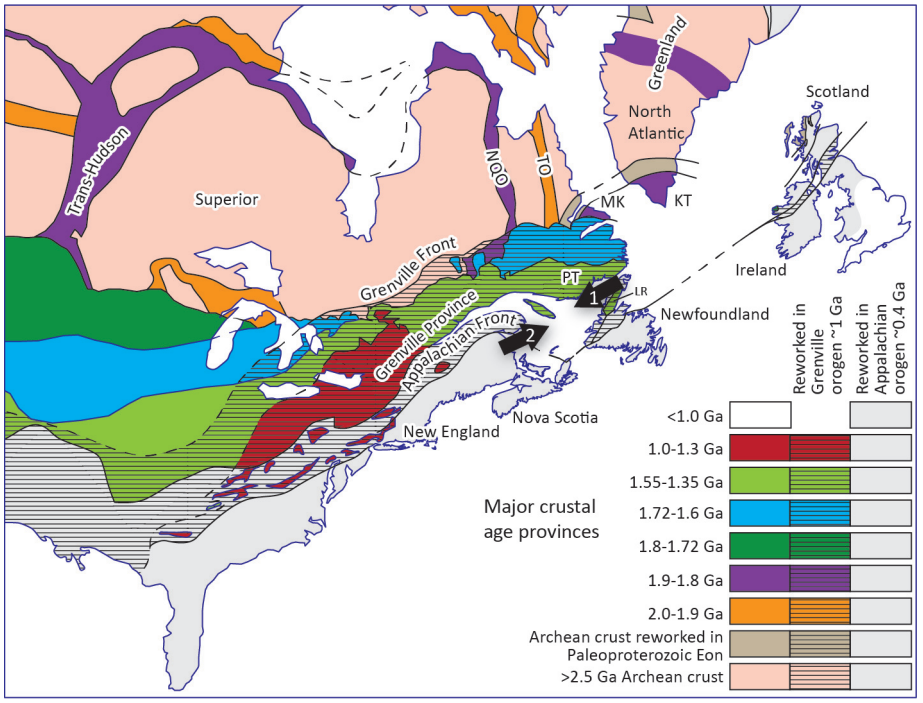

Fig. 2. Map showing major structural provinces which make up eastern Laurentia, based on data and interpretations of Whitmeyer and Karlstrom (2007), Nutman and others (2008), St. Onge and others (2009), Rivers (2009, 2015). KT, Ketilidian Orogen; MK, Makkovik Orogen; NQO, New Québec Orogen; TO, Torngat Orogen. Arrow 1 is transport direction for Goose Tickle Group detritus. Arrow 2 is transport direction for Long Point Group detritus.

peri-Laurentian Dashwoods block (fig. 1; Waldron and van Staal, 2001); although its basement is nowhere exposed, isotopic and zircon inheritance studies indicate a Laurentian affinity (Whalen and others, 1997; van Staal and others, 2007; but see Karabinos and others, 2017 for an alternative view). Terranes that originated outboard of the Laurentian margin contain units of exotic affinity and zircon populations derived from these terranes have age spectra indicative of Gondwanan, not Laurentian, sources (Macdonald and others, 2014; Waldron and others, 2014). The spectra typically lack the 1.0 Ga Grenville peak, which is typical of Laurentian detritus (for example, Cawood and others, 2007a; Waldron and others, 2008). They also contain prominent peaks between 550 and 650 Ma, typical of units derived from either the Brasiliano or Pan-African orogen of the Amazonian or West African craton respectively (for example, Waldron and others, 2014). Gondwanan units also typically contain grains with ages ranging from 2.0 to 2.2 Ga, derived from either the Eburnean Orogen of West Africa or Trans-Amazonia Orogen of Amazonia (for example, Pothier and others, 2015). These ages are typically absent in detritus derived from eastern Laurentia (Waldron and others, 2014).

Rift and Passive Margin Units

The oldest stratified rocks in western Newfoundland were deposited above Mesoproterozoic basement during several episodes of Neoproterozoic to early Cambrian rifting (Cawood and others, 2001). These events led to the opening of the Iapetus Ocean, the development of conjugate margins of Laurentia and Amazonia

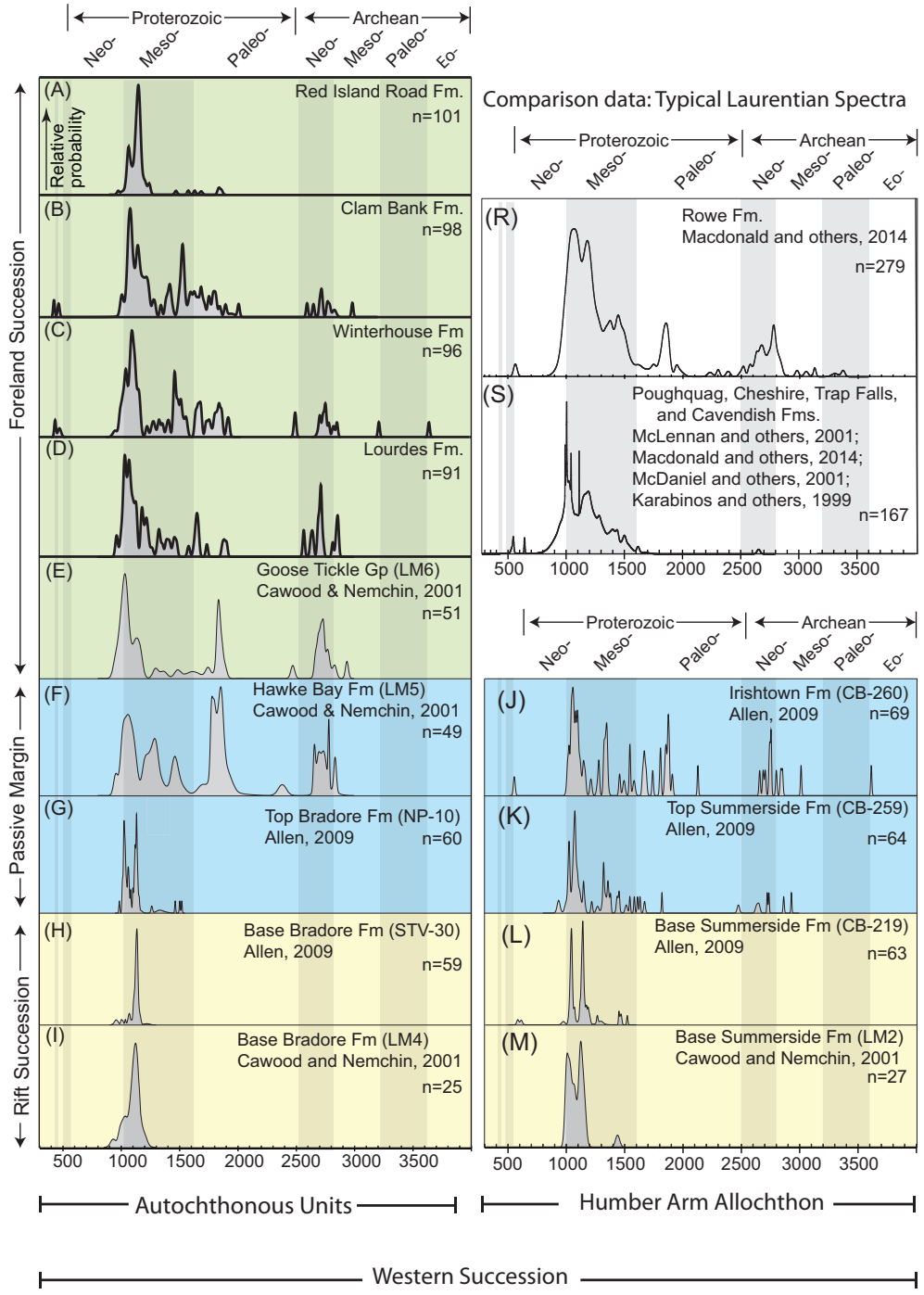

Fig. 3. *Continued.*

Fig. 3. Detrital zircon probability density functions for data from this study and previously published data. Vertical scale is in arbitrary units of relative probability density. This study: (A) Lourdes Fm. (NP007), (B) Winterhouse Fm. (NG024A), (C) Clam Bank Fm. (NG043), (D) Red Island Road Fm. (NP021), (E) American Tickle Fm. And, (F) Hawke Bay Fm. (Cawood and Nemchin, 2001), (G) Top Bradore Fm. and (H) base Bradore Fm. (Allen, ms, 2009). (I) Base Bradore Fm. (Cawood and Nemchin, 2001). (J) Irishtown Fm., (K) top Summerside Fm., and (L) base Summerside Fm. (Allen, ms, 2009). (M) Base Summerside Fm., (N) Blow Me Down Brook Fm., and (O) South Brook Fm. (Cawood and Nemchin, 2001). (P) Flat Brook Fm. (van Staal and others, 2013). (Q) inherited zircon in Notre Dame Arc (van Staal and others, 2007). (R) Rowe Formation (Macdonald and others, 2014). (S) Passive margin units in Quebec and New England. Sources include Poughquag quartzite (McLennan and others, 2001), Cheshire Formation (Macdonald and others, 2014), Trap Falls Formation (McDaniel and others, 1997), and Cavendish Formation (Karabinos and others, 1999).

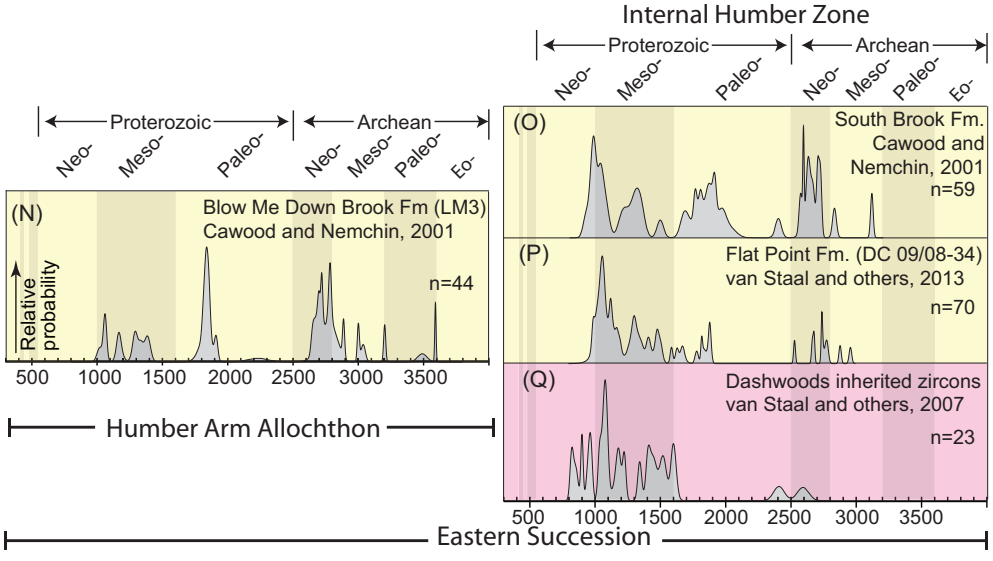

Fig. 3. *Continued.*

(Cawood and Williams, 1988; Cawood and others, 2001), and the rifting of crustal ribbons from both Laurentian (for example, Dashwoods block) and Amazonian margins (van Staal and others, 1998; Waldron and van Staal, 2001; van Staal and others, 2013).

Rifting generated a series of NE-striking and lesser NW-striking deep-seated extensional faults within the basin, forming grabens into which thick successions of clastic and local mafic volcanic rocks were deposited (Williams and Hiscott, 1987; Allen and others, 2010). Clastic units deposited into these basins include the autochthonous Cambrian Bradore Formation, and the correlative Summerside and Blow Me Down Brook formations (fig. 4) that are now exposed within the Humber Arm Allochthon (Palmer and others, 2001) (fig. 1). Within the metamorphosed eastern portion of the Humber Zone (fig. 1), the South Brook and Flat Point formations of the Fleur de Lys Supergroup represent equivalent synrift clastic units of the Laurentian margin. A dominantly carbonate middle Cambrian – Early Ordovician passive margin overlies the rift-related units. The autochthonous Hawke Bay and allochthonous Irishtown formations occur near the base of this succession and represent the only coarse-grained siliciclastic units within the passive margin succession (fig. 4). Thinly bedded high-energy carbonates of the middle to upper Cambrian Port au Port Group (Chow and James, 1987) overlie the Hawke Bay Formation, which in turn are overlain by massive, thick-bedded lower-energy limestone and dolostone of the Lower Ordovician St. George Group (Knight and James, 1987). The Cow Head Group represents deep-water lateral equivalents of this carbonate platform now exposed in the Humber Arm Allochthon (fig. 4).

Several previous U/Pb analyses of zircon in clastic portions of the rift and passive margin successions have been carried out (Cawood and Nemchin, 2001; Allen, ms, 2009; van Staal and others, 2013). We have divided these into eastern and western units, based on their interpreted depositional position relative to the Laurentian margin (fig. 3). Samples collected from the most westerly rift units display remarkably similar narrow age spectra dominated by strong peaks between 1.0 and 1.2 Ga (fig. 3). The basal Bradore Formation contains only one peak at 1.0 Ga; this narrow age spectrum is consistent with derivation from the immediate basement of the Grenville Orogen. The basal Summerside Formation and upper Bradore Formation are characterized by two distinct peaks at ~1.0 and 1.1 Ga, which we suggest might possibly delineate the Rigolet and Ottawan phases (Rivers, 2015) of the Grenville Orogeny respectively. These units also contain a small percentage (~15%) of older Mesoproterozoic grains, also consistent with derivation from the Grenville Province. In higher portions of the stratigraphic section, representing the passive margin succession, a broader range of ages is observed. The Hawke Bay and Irishtown formations both contain abundant Mesoproterozoic peaks between 1.2 and 1.6 Ga and very strong peaks at 1.85 Ga. These grains could be derived from either the Makkovik or associated Paleoproterozoic orogens (New Québec or Torngat) in the north or the Trans-Hudson region to the west. Both passive margin units have strong Archean signatures dominated by peaks at 2.7 to 2.8 Ga, typical of derivation from either the Superior or North Atlantic cratons.

Metamorphosed clastic units in the eastern Humber Zone (South Brook Formation) and Notre Dame Subzone (Flat Point Formation) (fig. 1), together with the structurally highest synrift unit of the Humber Arm Allochthon (the Blow Me Down Brook Formation), contain a much larger spread of ages compared to rift-related units deposited to the west, closer to the Laurentian margin (Bradore and Summerside formations) (fig. 3). Although these units still contain a significant population of Grenville zircon, forming peaks at 1.0 to 1.1 Ga, these peaks are diluted by the large proportion of Paleoproterozoic zircon within the spectra. The largest peak within the

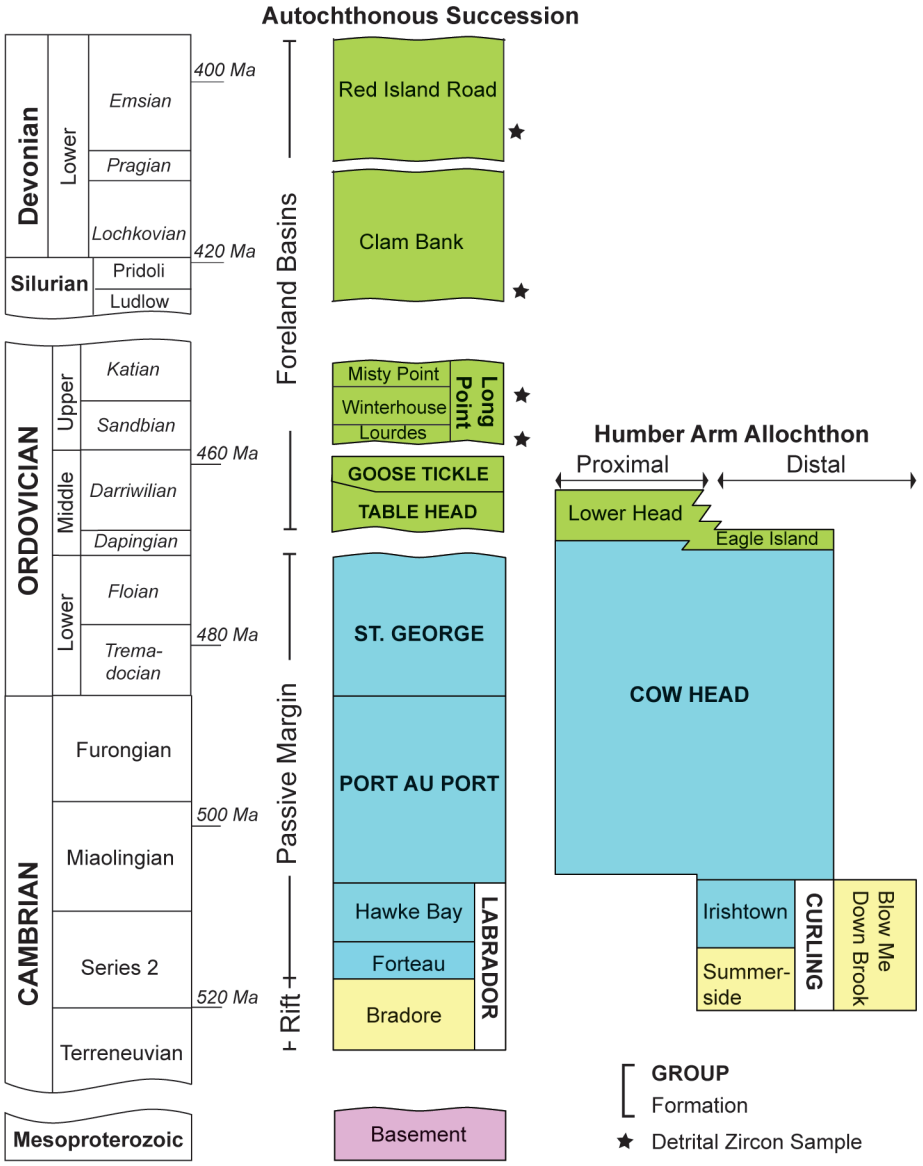

Fig. 4. Stratigraphic column showing units in western Newfoundland including autochthonous and allochthonous successions. Vertical scale is proportional to geologic age except at breaks marked by wavy lines. Colors consistent with figure 3.

Blow Me Down Brook Formation occurs at 1.85 Ga, while Paleoproterozoic ages in the Fleur de Lys Supergroup are dominated by 1.90 Ga peaks. These Paleoproterozoic peaks are consistent with derivation from Paleoproterozoic orogens either north (for example, Makkovik and/or Ketilidian orogens) or west (for example, Trans-Hudson Orogen) of the basin. Archean grains are dominated by Neoarchean detritus with strongest peaks ranging from 2.6 to 2.8 Ga. Smaller, but significant Mesoarchean peaks are observed while approximately 7 percent of grains in the Blow Me Down Brook

Formation have Paleoarchean ages. Archean ages suggest derivation from either the Superior or North Atlantic craton.

Ordovician Taconic Orogeny and Foreland Basin

The Ordovician Taconic Orogeny involved the collision of Laurentia with an arc developed at an east-dipping subduction zone (Waldron and van Staal, 2001; van Staal and others, 2009), and westward emplacement of allochthons (Williams and Stevens, 1974; St. Julien and Hubert, 1975) on top of the Laurentian margin. Continental rift, and passive margin units are exposed in a series of stacked thrust sheets within the Humber Arm Allochthon (Waldron and others, 2003). Highest thrust sheets within the allochthon contain ~508 to 485 Ma (Dunning and Krogh, 1985; Jenner and others, 1991) suprasubduction zone ophiolites which represent arcs (Dewey and Bird, 1971; Dewey and Casey, 2013) formed within the Iapetus Ocean. Structurally below the allochthons, and within the developing pro-arc foreland basin, deep-seated normal faults were activated in response to flexure of the lower Laurentian plate during orogenic loading and slab pull (Bradley and Kidd, 1991).

The St. George unconformity, at the top of the autochthonous passive margin, represents the transition to a tectonically active basin (Knight and others, 1991) (fig. 4). The unconformity is overlain by the dominantly carbonate Table Head Group (Stenzel and others, 1990) which is in turn stratigraphically overlain by sandstone and siltstone of the Goose Tickle Group. Overall basin geometry and ophiolitic detritus within turbiditic sandstone units (Stevens, 1970) indicate that the Goose Tickle Group formed in a foreland-basin setting, sediments being derived from the Newfoundland portion of the orogen (White and others, 2019). SW-directed paleocurrent indicators (Quinn, ms, 1992; Batten Hender and Dix, 2008) also imply that sediments were sourced axially, from the northeast, consistent with northeastward thickening of the Goose Tickle Group offshore (White and others, 2019).

Only one published work by Cawood and Nemchin (2001) records U/Pb analyses of zircon from the Goose Tickle Group (fig. 3). The age spectrum is dominated by a strong peak at 1.05 Ga. This peak and older, smaller Mesoproterozoic peaks are consistent with ages of units in local Grenvillian basement. A strong peak at 1.85 Ga is consistent with unit ages within any of the eastern Laurentian Paleoproterozoic orogens (Trans-Hudson, Makkovik or New Québec-Torngat). A strong Archean signature, dominated by 2.70 Ga grains, is also consistent with the age of units within the Superior and North Atlantic cratons. The presence of ophiolitic detritus within the Goose Tickle Group (Hiscott, 1984; Quinn, ms, 1992) indicates that it is more likely derived from recycling of clastic units within the Humber Arm Allochthon, rather than being derived from Laurentian basement units.

Late Ordovician Long Point Group

The Long Point Group, comprising the Lourdes, Winterhouse and Misty Point formations, represents the Late Ordovician foreland basin succession in western Newfoundland. The Lourdes Formation, a 75 m thick unit of shallow-marine limestone, disconformably overlies the Goose Tickle Group and represents the base of the Long Point Group. The depositional age for the Lourdes Formation is constrained by Upper Ordovician (Sandbian) conodonts (*Baltoniodus gerdae* Biozone) and graptolites (*Diplograptus multidens* Biozone) (Bergström and others, 1974). Batten Hender and Dix (2008) describe the formation as a narrow, high-energy, mixed siliclastic-carbonate ramp succession. The Lourdes Formation is gradationally overlain by thin-to medium-bedded fine-grained sandstone and shale units of the Winterhouse Formation, interpreted to represent a storm-dominated shelf assemblage (Quinn and others, 1999). Graptolite species *Climacograptus spiniferus* and *Geniculograptus pygmaeus* indicate a Late Ordovician (Katian) depositional age (Quinn and others, 1999). These rocks

are gradationally overlain by medium- to coarse-grained red sandstone units of the Misty Point Formation interpreted to have been deposited in a marginal marine to terrestrial setting (Quinn and others, 1999). The presence of Ordovician brachiopods *Sowerbyella sericea* and *Rafinesquina deltoidea*, associated with species of *Trigrammaria*, also indicate a Katian age of deposition (Quinn and others, 1999). No previous geochronologic work has been carried out on any units within the Long Point Group.

Seismic horizon mapping (White and others, 2019) indicates that the narrow Lourdes shelf is restricted to southern portions of the basin, and that the Lourdes Formation filled residual topography that remained after the Taconic Orogeny. The remainder of the Long Point Group thickens dramatically southwards, indicating basin subsidence as a result of loading in the Québec Appalachians where Taconic arc-continent collision continued into the Late Ordovician (White, ms, 2017). During this interval, subduction polarity reversal had already occurred in central Newfoundland (Zagorevski and others, 2009), leading to westward subduction beneath the developing orogen, placing the Long Point Group in a retro-arc setting (Naylor and Sinclair, 2008). These observations, together with NE-directed paleocurrent data (Batten Hender and Dix, 2008) suggest that the Long Point Group was loaded along-margin from Québec, where arc-continent collision above an east-dipping subduction zone continued into the Late Ordovician (White and others, 2019).

Silurian to Early Devonian Clam Bank Formation

The Clam Bank Formation unconformably overlies the Long Point Group (fig. 4). This unconformity (the Clam Bank unconformity) is significant, removing the majority of the Silurian system in western Newfoundland; however, it is not exposed anywhere on land because the units above and below are juxtaposed by a fault at their only exposed contact. The lowest units in the Clam Bank Formation consist of red and green thin-bedded calcareous mudstone and siltstone interlayered with noncalcareous siltstone and sandstone. These rocks are interpreted to have been deposited in a shallow-marine to terrestrial environment (Burden and others, 2002). A conodont assemblage of *Ozarkodina remscheidensis eosteinhornensis* and *O. remscheidensis* ssp. (Burden and others, 2002) indicates a maximum depositional age of Pridoli to Lochkovian for this portion of the Clam Bank Formation. A second unconformity above this mixed lower portion marks the transition to a dominantly siliciclastic succession of coarse-grained sandstone, interpreted to have been deposited in a terrestrial environment (Burden and others, 2002).

The Clam Bank unconformity correlates in timing with the protracted Salinic Orogeny (455–422 Ma; Dunning and others, 1990; Cawood and others, 1994; van Staal and others, 2009), resulting from collision of Ganderian microcontinents at a west-dipping subduction zone along the composite Laurentian margin (van Staal and others, 1998; van Staal and others, 2009; Waldron and others, 2019). The foreland basin, forming on top of the Laurentian plate, likely underwent significant exhumation towards the end of this episode as Ganderian microcontinents were underthrust at the margin. The Clam Bank Formation was deposited as a result of later erosion of the Salinic Orogen into a retro-arc foreland basin (White and others, 2019).

Early Devonian Red Island Road Formation

The Red Island Road Formation, exposed only offshore on Red Island (fig. 1), is the youngest foreland basin succession in western Newfoundland, based on palynomorphs discovered by Quinn and others (2004), placing the Red Island Road Formation in the Emsian *Emphanisporites annulatus – Camarozonotriletes sextantii* Assemblage Zone. The unit is interpreted to overlie the Clam Bank Formation (Quinn and others, 2004), although the contact is not exposed on land. The Red Island Road Formation mainly consists of cobble to boulder conglomerate with a matrix of coarse-grained

sandstone. Clasts within the conglomerate include a mix of lithologies including sedimentary, metasedimentary and igneous; felsic volcanic rocks make up a large proportion of the clasts, for which no local source is known. The formation has been interpreted as a high-gradient gravel river bed deposit (Quinn and others, 2004).

The Early Devonian Acadian Orogeny in Newfoundland, occurring from ~ 420 to 400 Ma (van Staal and others, 2009), overlaps with deposition of the Red Island Road Formation. The orogeny has been attributed to the accretion of Avalonia to Laurentia (Bird and Dewey, 1970; Bradley, 1983; van Staal and others, 2009) via west-dipping subduction (Waldron and others, 1996; Murphy and others, 1999; van Staal and others, 2014), implying that the Acadian foreland basin developed as a retro-arc basin (White and others, 2019); the Red Island Road Formation filled this Early Devonian basin. In western Newfoundland, the orogeny led to reactivation and inversion of earlier Taconic and Neoproterozoic basement faults and the uplift of basement massifs, including the Long Range and Indian Head Inliers (White and Waldron, 2019).

U/Pb geochronology

We chose samples from four foreland basin units for detrital zircon geochronology by Laser Ablation Multicollector Inductively Coupled Plasma Mass -Spectrometry (LA-MC-ICP-MS): the Lourdes, Winterhouse, Clam Bank and Red Island Road formations (fig. 4). Geographic and stratigraphic sample locations are shown in figures 1 and 4 respectively. Samples were chosen based on fossil control, where available, in order to constrain depositional age. Coarse-grained sandstone units were collected, where possible, to maximize the likelihood of obtaining zircon of suitable size for analyses. One sample of a typical rhyolite boulder from a conglomeratic bed within the Red Island Road Formation was collected for U-Pb age dating of zircon using Chemical Abrasion Thermal Ionization Mass Spectrometry (CA-TIMS). Cathodoluminescence (CL) and backscattered electron (BSE) images of representative zircon grains are shown in figure 5. Details of sample processing, analytical methods, graphical techniques, and full tables of results are given in the Appendix in tables A1-A4. Plots were prepared using Isoplot (Ludwig, 2012) and software from the Arizona LaserChron Center (Gehrels and others, 2006).

Results

Lourdes Formation

The sample of the Lourdes Formation (NP007A) was collected on Long Point (fig. 1). Bedding in this location dips shallowly to moderately northwest and the rocks have not been penetratively deformed. Biostratigraphically significant fossils mainly occur in the middle unit (Black Duck Member) of the Lourdes Formation and include Upper Ordovician (Sandbian) conodonts of the *B. gerdae* Biozone (Bergström and others, 1974) and graptolites of the *D. multidens* Biozone (Bergström and others, 1974). Specific diagnostic species of conodonts include *Appalachignathus delicatulus* (Bergström and others, 1974), *Belodina* sp., *Periodon* sp., and *Walliserodus ethingtoni* (Fåhraeus, 1966). Our sample was taken from the overlying Beach Point Member because it contained a significant amount of clastic material. The age is constrained, by these underlying fossils and those found in the overlying Winterhouse Formation, as Sandbian or Late Ordovician.

The sample of the Lourdes Formation was collected from a thin laminated bed of very fine-grained calcareous sandstone and limestone, the coarsest material available. The outcrop was a medium to thick bedded succession of burrow-mottled limestone, punctuated by a few thin layers of very fine-grained calcareous sandstone. The sample collected for analysis was a well sorted, subrounded to subangular, very fine-grained calcarenite (fig. 6A) with ~50 percent carbonate material. The carbonate material is

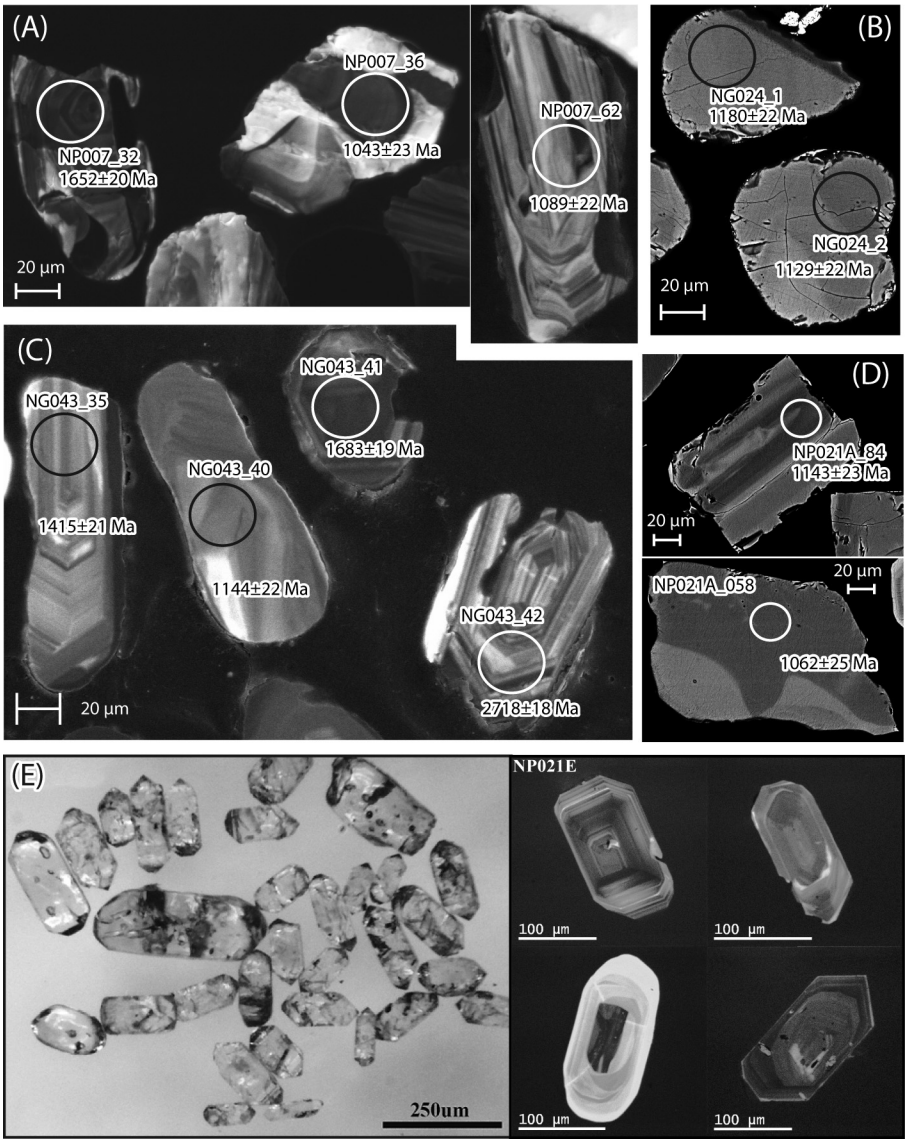

Fig. 5. Cathodoluminescence (CL) and backscattered electron (BSE) images of representative zircons from this study. (A) CL images of representative zircons from sample NP007A. Zircon 32 displays a magmatic, oscillatory zoned core with a metamorphic overprint manifested as an irregular rim showing sector zoning. Metamorphic grain 36 displays sector zoning. Grain 62 demonstrates oscillatory zoning typical of elongate magmatic grains with ages of ~ 1.1 Ga. (B) Backscattered electron images of zircons from sample NG024A showing low contrast wavy flow zoning. (C) CL images of selected zircons from sample NG043A. Magmatic zircons 35 and 42 display oscillatory zoning. Grain 40 displays broad sector zoning typical of metamorphic zircons in the sample. (D) Backscattered electron images of grains from sample NP021A. Metamorphic grain 84 displays parallel sector zones; metamorphic grain 58 shows wavy flow zoning. (E) Zircon from rhyolite boulder NP021E; left - transmitted light; right - cathodoluminescence image.

mainly peloids and sparry calcite cement. The clastic component is feldspathic litharenite, containing a mixture of quartz, polycrystalline quartz, lithic fragments and alkali feldspar.

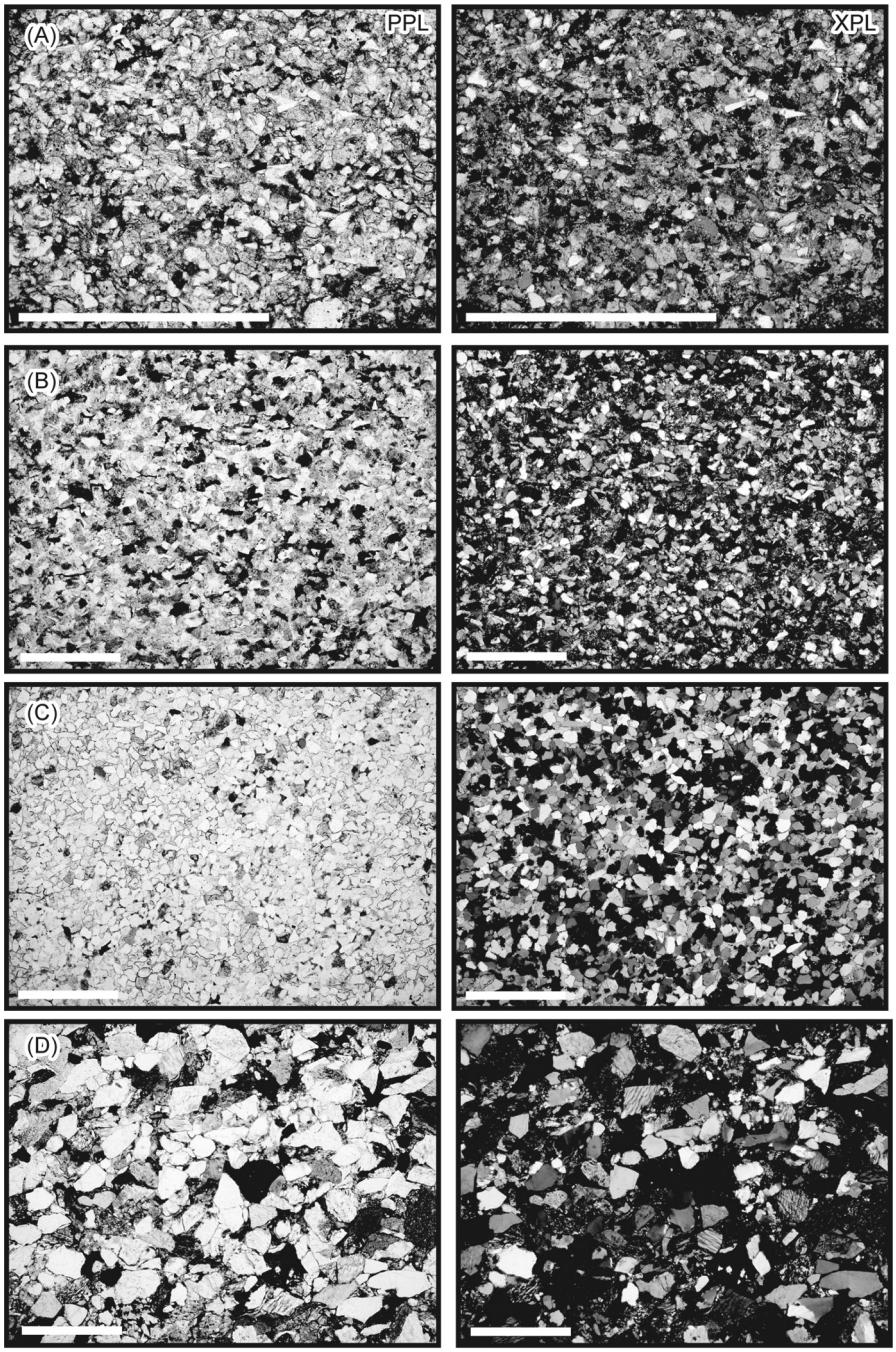

Fig. 6. Photomicrographs of sampled foreland basin units including: (A) Lourdes Formation; (B) Winterhouse Formation; (C) Clam Bank Formation; (D) Red Island Road Formation. Scale bars 1 mm. PPL - plane polarized light; XPL - crossed polars.

Zircon within the sample is subangular to surrounded and displays moderate sorting, ranging in size from 40 to 240 μm. Although grains vary in shape from equant to elongate, larger grains (>150 μm) have an aspect ratios ranging from 1:3 to 1:5. Most zircon displays typical metamorphic zoning including wavy flow, sector and banded zoning. Of the 130 zircon grains analyzed, 91 grains are less than 10 percent discordant. Of the concordant grains almost 80 percent are Mesoproterozoic (fig. 3). The largest proportion of analyses falls between 0.95 and 1.3 Ga, comprising over 50 percent of the grains. The largest peak within this range occurs between 1.0 and 1.1 Ga, a typical age range for zircon derived from the Grenville Orogen. Oscillatory zoning is typical of elongate, larger magmatic zircons with an age of ~ 1.1 Ga. A significant number of zircon grains, 26 percent, are spread throughout the earlier Mesoproterozoic to Paleoproterozoic, between approximately 1.3 and 2.0 Ga, with the largest peak within this range at ~ 1.65 Ga. A 1.85 Ga peak, generally typical of Laurentian zircon (Cawood and Nemchin, 2001), is absent. About 21 percent of grains give Archean ages from 2.5 to 2.9 Ga, with the largest peak at ~2.75 Ga, a common age for Laurentian zircon derived from either the Superior or North Atlantic craton (Calvert and Ludden, 1999; Corfu and Lin, 2000; Downey and others, 2009). A conspicuous gap between ~2.0 to 2.5 Ga is observed (fig. 3), which is also typical of zircon populations derived from eastern Laurentia (Cawood and Nemchin, 2001; Waldron and others, 2008).

Winterhouse Formation

We collected the sample of the Winterhouse Formation (NG024A) from the stratigraphically highest portion of the Formation, near the contact with the stratigraphically overlying Misty Point Formation. This location is the waterfall reference section of Quinn and others (1999) (fig. 1), which has a well constrained depositional age based on graptolite species *C. spiniferus* and *G. pygmaeus*, placing this locality in the lower part of the *pygmaeus* Zone, indicating a Late Ordovician, Katian age.

The sample was collected from an outcrop of parallel-laminated, thin-bedded sandstone. It is a very fine-grained lithic arkose, containing abundant alkali feldspar and scarce plagioclase, together with a variety of plutonic, sedimentary, and volcanic rock fragments, and lesser amounts of quartz (fig. 6B). Feldspars and volcanic rock fragments are strongly altered to clay minerals. The sand was originally probably well sorted, but original porosity has been occluded by compaction of rock fragments, strongly modifying the grain shapes.

Zircon within the Winterhouse sample is moderately to well-sorted with grains ranging in size from 50 to 200 μm. The average grain size is 100 μm. Zircon is predominantly rounded; angular grains are clearly broken pieces of larger zircon. Grains display both equant and elongate shapes, about 65 percent of grains having aspect ratios ~ 1:2.

A total of 96 out of 125 analyzed zircon grains were less than 10 percent discordant within the Winterhouse Formation. Approximately 43 percent of zircon grains range from 0.95 to 1.2 Ga, the largest peak within this range occurring at 1.1 Ga, typical of local Grenvillian units. A significant percentage of analyses, about 42 percent, are of earlier Mesoproterozoic to Paleoproterozoic age, ranging from 1.3 to 2.0 Ga. In common with the Lourdes Formation, a conspicuous gap is observed between 2.0 and 2.5 Ga and a small proportion of analyses (11%) give Archean ages ranging from 2.5 to 2.9 Ga with the largest peak at 2.75 Ga. These age populations are similar to those observed in the Lourdes Formation (fig. 3). Two older Archean grains at 3.2 and 3.6 Ga are present in the Winterhouse Formation; comparable grains are not observed in any other foreland basin unit. Two grains have much younger Paleozoic ages. A grain with an age of 470 Ma is consistent with the timing of ophiolite obduction onto the Laurentian margin and may represent a metamorphic age associated with this Taconic

event. The other grain, although having an anomalously young $^{206}Pb/^{238}U$ age of 435 Ma, younger than the depositional age, is 7 percent discordant and has a $^{207}Pb/^{206}Pb$ age of 465 Ma. The grain most likely suffered lead loss. The $^{207}Pb/^{206}Pb$ age is consistent with metamorphism during Taconic orogenesis. There is no clear correlation with age and zircon morphology.

Clam Bank Formation

The sample of Clam Bank Formation (NG043A) was taken in the footwall of the Round Head thrust where bedding is steep to overturned (fig. 1). There are no fossils in this portion of the Clam Bank succession; however, fossils, including a conodont assemblage of *Ozarkodina remscheidensis eosteinhornensis* and *O. remscheidensis* ssp. from the marine portion of the Clam Bank Formation (Burden and others, 2002), a few meters above the sampled bed, indicate a minimum depositional age of Pridoli to Lochkovian.

We took the sample from a thick overturned bed of coarse-grained, well sorted, sandstone near the stratigraphic base of the exposed on-land section of Clam Bank Formation. The sample is a subarkosic arenite with carbonate cement (fig. 6C). Grains are predominantly monocrystalline quartz with minor feldspar (mostly microcline) and rare lithic fragments.

Zircon is rounded and well-sorted in the sample and has an average grain size of ~100 μm. The majority of zircon is metamorphic, displaying sector and flow zoning. Magmatic zircon has well preserved oscillatory zoning. Zircon analyses from the Clam Bank Formation generate a probability density function similar to those of both the Winterhouse and Lourdes formations (fig. 3). The distribution includes 98 analyses which were less than 10 percent discordant out of 137 total analyses. Approximately 45 percent of analyzed concordant grains are within the range of 1.0 to 1.2 Ga and the largest peak occurs at 1.1 Ga, similar to both the older formations. A major proportion of the grains (43 %) span the age range 1.2 to 2.0 Ga. There is a complete absence of grains between 2.0 and 2.6 Ga, also similar to the Winterhouse and Lourdes formations. A smaller, but still significant proportion of grains occur from 2.6 to 3.0 Ga, with the largest peak at 2.75 Ga. Only two grains yielded Paleozoic ages of 425 and 465 Ma. The 425 Ma age is very close to the depositional age of the unit while the 465 Ma zircon is consistent with derivation from a Taconic source. There is no obvious correlation between age and zircon morphology.

Red Island Road Formation

The Red Island Road Formation was sampled (NP021A) on Red Island, the only place the unit is exposed (fig. 1). The beds are subhorizontal, dipping very gently (~05°) north. The depositional age of the unit is constrained by biostratigraphically significant palynomorphs above the sampled location, which place the unit in the Emsian *Emphanisporites annulatus – Camarozonotriletes sextantii* Assemblage Zone (Quinn and others, 2004).

We sampled a bed of medium-grained sandstone interlayered between thick beds of cobble to boulder conglomerate, in which rhyolite clasts are common (fig. 5D). The sandstone is a moderately sorted, subangular, feldspathic litharenite, with subequal amounts of quartz, metamorphic rock fragments, and feldspar (mainly perthitic). As in the case of the Clam Bank sample, compaction of lithic fragments has modified the original texture.

We also collected a rhyolite boulder (~ 30 cm in diameter) from a conglomeratic bed within the Red Island Road Formation (NP021E) (Location: fig. 1). This boulder is representative of the most common lithology of cobbles and boulders within the conglomerate and all rhyolites within the unit are petrographically similar. The sample

is a porphyritic rhyolite, with phenocrysts of quartz and potassium feldspar in an aphanitic matrix.

Zircon in NP021A is moderately sorted with an average grain size of ~140 μm. Mesoproterozoic grains range from angular to rounded, many grains being clearly broken, having cuspate/concave boundaries. Grains display both oscillatory magmatic zoning and sector and wavy flow zoning typical of metamorphic zircon. The probability density function for zircon analyses from the Red Island Road Formation notably differs from the distributions of the three younger units (fig. 3). Of the 101 concordant analyses, 93 had Mesoproterozoic ages between 950 Ma and 1.2 Ga. The largest peak is at 1.15 Ga. Only four analyses have ages between 1.5 to 1.7 Ga and three other zircon grains make a small peak at approximately 1.85 Ga. The handful of Paleoproterozic grains are generally smaller, equant, and rounded and display sector zoning typical of metamorphic zircon. There were no Archean grains, in contrast to all other foreland basin units.

Two of the four TIMS analysis carried out on the rhyolite boulder from the Red Island Road Formation (Z2, Z4) are concordant (fig. 7E). The other two are significantly discordant, having much older $^{207}Pb/^{206}Pb$ ages than the $^{206}Pb/^{238}U$ ages. This is indicative of an inherited zircon component in at least one crystal of each fraction. Two of the concordant analyses have $^{206}Pb/^{238}U$ ages of 421 +/− 1.8 and 421 +/− 2.1 Ma, each at 2σ. The weighted average $^{206}Pb/^{238}U$ age is 421 +/−1.3 Ma (Isoplot, 95% confidence interval, MSWD = 0.44). This age is in the Pridoli Epoch (latest Silurian) using the timescale of Melchin and others (2012).

K-S Test

The Kolmogorov-Smirnoff (K-S) two-sample test is based on measuring the maximum difference (D) between each pair of cumulative distribution functions (CDFs). It can provide a useful objective measure of whether two samples could have come from the same statistical population (Vermeesch, 2018), although caution is required in inferring similarities and differences between geological sources from these statistical similarities, as hydrodynamic and other processes unrelated to provenance can influence the age-distribution of detrital zircon (Ibañez-Mejia and others, 2018). Figure 8 displays the results of the K-S test, for each of the four sampled foreland basin units in this study. Results are expressed as a value P which is the probability that the observed D values could result from random sampling of a single population. High values of P indicate that the samples could have been drawn from the same source population. For the three oldest samples, the Lourdes, Winterhouse and Clam Bank formations, $D < D_{crit}$ for all pairs and we therefore accept the null hypothesis that these samples could have been derived from the same population. This agrees with our qualitative observations from the PDFs, which are all similar to one another. The similarity of the detrital zircon age-distributions, despite the petrographic contrasts between the three samples, suggests that hydrodynamic factors discussed for fluvial sediments by Ibañez-Mejia and others (2018) have not seriously influenced the results. The cumulative probability difference between these older units and that of the youngest Red Island Road Formation is much greater than D_{crit} (despite the petrographic similarity between the Winterhouse and Red Island Road samples). We therefore reject the null hypothesis and interpret that this youngest unit was not derived from the same population as the older foreland units. This also agrees with our earlier qualitative interpretations, that the Red Island Road Formation has a distinctly different detrital zircon age spectrum from all other units analyzed in this study.

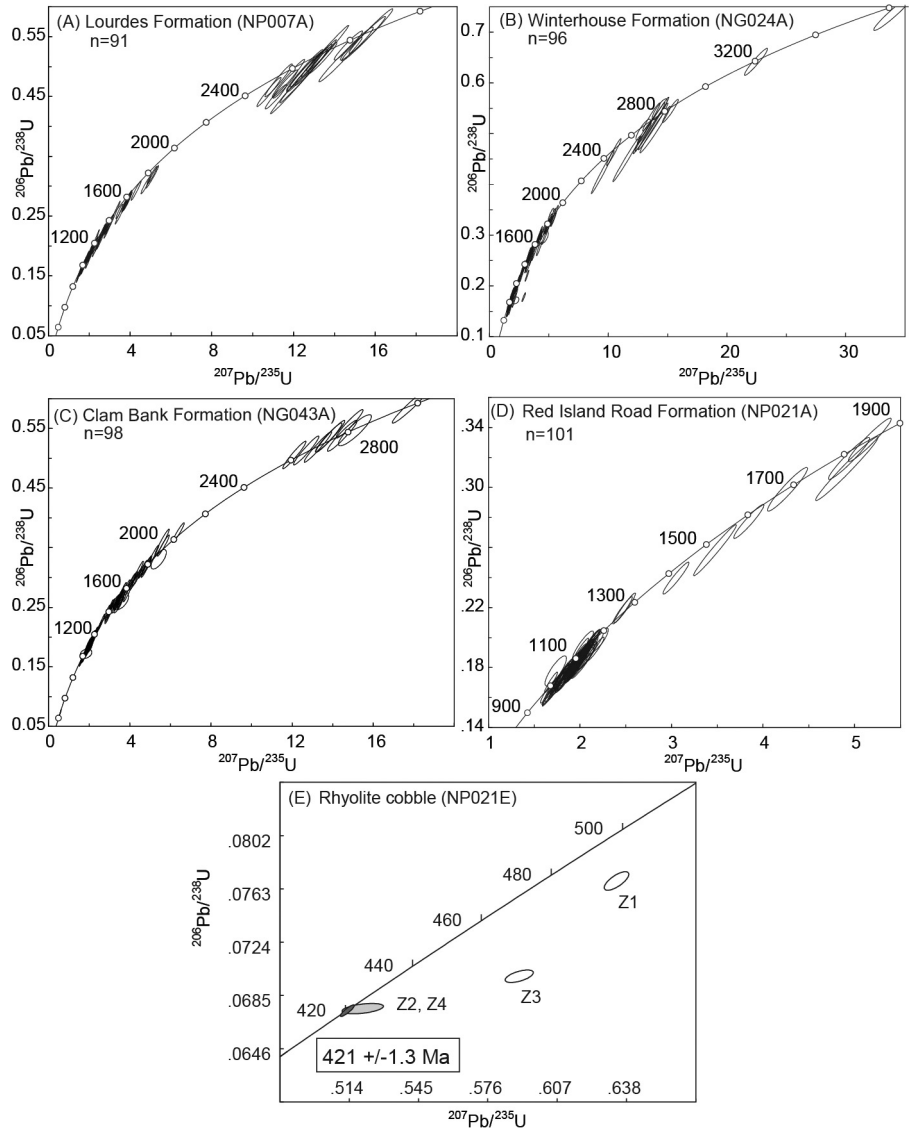

Fig. 7. U-Pb concordia plots for detrital zircon data from this study including: (A) NP007 (Lourdes Formation), (B) NG024A (Winterhouse Formation), (C): NG043 (Clam Bank Formation), (D) NP021 (Red Island Road Formation), and (E) NP021E (zircon from rhyolite boulder). Ellipses represent 2σ uncertainties.

DISCUSSION

In this section we discuss new detrital zircon data from this study in context of previously published data and a current understanding of tectonic evolution of the northern Appalachians.

Previously published detrital zircon data from the Goose Tickle Group (Cawood and Nemchin, 2001) demonstrate age populations that can be explained by derivation from siliciclastic units preserved in the Humber Arm Allochthon (fig. 3). Although Mesoproterozoic peaks between 1.2 and 1.7 Ga are diminished, relative to continental

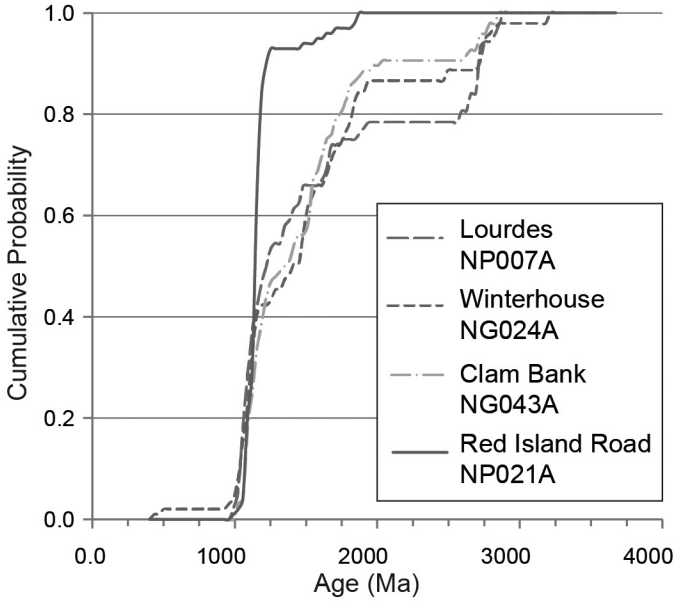

	Lourdes NP007A	Winter-house NG024A	Clam Bank NG043A	Red Island Road NP021A
Lourdes NP007A		0.535	0.497	0.000
Winterhouse NG024A	0.535		0.833	0.000
Clam Bank NG043A	0.497	0.833		0.000
Red Island Road NP021A	0.000	0.000	0.000	

Fig. 8. Detrital zircon cumulative density plots and results of the K-S test expressed as probability value P for all pairs of samples analyzed in this study.

margin units preserved in the allochthon, a large Paleoproterozoic peak is present at 1.85 Ga, similar to that observed in the most distal rift and passive margin units. Previous interpretations, based on paleocurrent analyses (Quinn, ms, 1992) and geochemical work on detritus (Hiscott, 1978), also point towards derivation from the Humber Arm Allochthon immediately east of the basin. However, thickness data derived from seismic reflection profiles by White and others (2019) indicate that the succession is derived from more northern regions of the Newfoundland orogen.

The overlying Lourdes, Winterhouse and Clam Bank formations all display probability density plots which are very similar to one another and, using the results from the K-S test, we accept the null hypothesis that these three samples could have been derived from the same source region. We did not perform the K-S test using the Goose Tickle Group due to the great disparity in the number of analyses relative to our samples. Although zircon ages from these units are similar to those observed in the Goose Tickle Group and siliciclastic units of the Humber Arm Allochthon, the proportions of ages (that is relative peak heights) differ drastically. The most obvious

difference is the conspicuously low abundance of Paleoproterozoic grains with ages of ~ 1.85 Ga, which are abundant in the Goose Tickle Group. In the Lourdes Formation the 1.85 Ga peak is absent (fig. 3). This diminished/absent peak indicates a major shift in provenance during development of the Long Point Group basin.

This shift in provenance coincides with a major shift in Late Ordovician basin geometry, recognized by White and others (2019) who show that prior to deposition of the Long Point Group, the foreland basin thickened northward and eastward, implying loading by the northern Newfoundland segment of the orogen. A dramatic shift, to a southward-thickening basin, followed during Late Ordovician deposition of the Long Point Group where it is interpreted that loading along the southern margin of the basin by Taconic allochthons, now preserved on the Gaspé Peninsula in Québec, generated the basin into which the Long Point Group was deposited.

Compositionally, the Winterhouse and Misty Point formations are similar to the Goose Tickle Group. Batten Hender and Dix (2008) show that ratio ranges of Y/Ni and Cr/V for all three units are similar, suggesting all three units are derived from sources including ophiolites (Hiscott, 1984; Quinn, ms, 1992). The prominent unidirectional northeast-directed paleocurrent indicators, and compositional similarities indicate that the Winterhouse and Misty Point formations were derived from the allochthons in Québec, rather than Newfoundland (fig. 2, arrow 2).

Although no detrital zircon studies have been carried out on continental margin clastics within allochthons on the Gaspé Peninsula, data have been collected farther south, in New England (McLennan and others, 2001; Macdonald and others, 2014; Macdonald and others, 2017). The probability density plots of Laurentia-derived zircon from the Paleozoic metasedimentary rocks in New England all display a much diluted Paleoproterozoic (~1.85 Ga) peak, similar to the relatively small 1.85 Ga peak within the Long Point Group and Clam Bank Formation in Newfoundland. Other studies which look at zircon in the Cambrian passive margin units in New England (fig. 3S) demonstrate a complete absence of Paleoproterozoic ages (Gaudette and others, 1981; McDaniel and others, 1997; McLennan and others, 2001). We interpret that the decrease in 1.85 Ga ages within the Upper Ordovician to Early Devonian (fig. 3) foreland basin succession of western Newfoundland signals the transition from a basin filled by erosion of the Humber Arm Allochthon to a basin filled by southerly derived detritus from the Québec and New England Appalachians (fig. 2, arrows 1 and 2).

There are no detrital zircon data from precise correlatives of the Long Point Group in central or eastern Newfoundland. However, Waldron and others (2012) report a distribution from the slightly younger (Katian) Point Leamington Formation in the Badger Group of central Newfoundland. The overall abundance of Mesoproterozoic and older zircon is similar to that of the Long Point Group, but the sample contains a large population of Early Ordovician grains, interpreted as derived from the Notre Dame Arc, preserved in the Peri-Laurentian Notre Dame Subzone immediately west of the sample location. The contrasting scarcity of Ordovician zircon in samples from the Long Point Group implies that the Taconic Orogen on the Laurentian margin was still a significant topographic divide in Late Ordovician time. This divide must have persisted at least until the deposition of the Pridoli to Lokhovian Clam Bank Formation, which also lacks Ordovician zircon.

The youngest foreland basin succession, the Red Island Road Formation (fig. 4), has a distinctly different age distribution compared to those from older foreland units, with only one large peak in the population at 1.15 Ga, a handful of Mesoproterozoic and Paleoproterozoic grains, and a complete absence of all other populations (fig. 3). Combined with the results from the K-S test (fig. 8), this indicates that the Red Island Road Formation is not derived from the same source

region as the older foreland units. Clasts of high grade metamorphic and felsic volcanic rock, documented in the provenance study of Quinn and others (2004), also suggest that sources other than earlier foreland basin and platform units provided detritus to the unit.

The most striking observation is the similarity of the Red Island Road Formation spectrum to those of autochthonous Bradore Formation (fig. 3). This unit also displays a very restricted spectrum of ages, the majority of which combine to form a strong 1.15 Ga peak, consistent with derivation from local Grenvillian basement. These observations may be explained by orogen development during the Acadian Orogeny. White and Waldron (2019) demonstrate that Middle Ordovician and Neoproterozoic basement-involved faults were reactivated and inverted during the Acadian Orogeny, uplifting basement massifs and transporting large, basement-cored fault-propagation folds up to 12 km towards the west. A strong influx of Grenvillian detritus was likely shed from Acadian basement uplifts into developing Acadian foreland basins suggesting that these massifs formed major topographic highs which are preserved today in the Long Range Mountains in Newfoundland.

Although the detrital zircon in the sandstone sample can all be derived from the Grenville Province, the larger rhyolite cobble within the conglomerate facies has an age of 421 +/− 1.3 Ma (fig. 7E). No local sources for Silurian felsic volcanic units are known in this region, although Heaman and others (2002) note the occurrence of Silurian (430.5+/− 2.5 Ma) mafic volcanic units in the Long Range Inlier. In southwestern Newfoundland, the Silurian La Poile Group (fig. 1) contains felsic volcanic rocks, dated at 420 +8/−2 Ma (Dunning and others, 1990), deposited on Precambrian basement (O'Brien and O'Brien, 1989). Bashforth (ms, 1995) and Quinn and others (2004) suggested, based on lithological matching, that these volcanic units sourced cobbles within the Red Island Road Formation. Quinn and others (1999) also suggest that other regions within the Notre Dame subzone may have sourced the conglomerate. Although both the La Poile Group and Notre Dame Subzone can explain Silurian volcanic cobbles, the prevalence of Grenvillian detrital zircon is not well explained by derivation from either of these terranes as neither of these regions has any exposure of Grenville basement.

We should also consider terranes presently outside Newfoundland as potential sources because the relative positions of source terranes have been modified by later transcurrent movement. A restoration of Appalachian terranes prior to Carboniferous motion by Waldron and others (2015) shows some outboard terranes shifted ~250 km NE of their present-day positions; Cape Breton Island lies directly east of the present position of the Port au Port Peninsula. Two main possibilities for Silurian source terranes exist there. First, the Aspy terrane (fig. 1) contains abundant plutons which are age equivalent (Lin and others, 2007) and compositionally similar to rhyolitic cobbles within rocks of the Red Island Road Formation. However, the Peri-Gondwanan Aspy terrane displays a wide range of ages. Metasedimentary units have detrital zircon ranging in age from 573 to 1520 Ma and igneous units range in age from 428 to ~ 620 Ma (Lin and others, 2007). One might expect, if detritus were derived from here, a larger span of detrital zircon ages within the Red Island Road Formation. The second option is the Blair River Complex in northern Cape Breton Island (fig. 1), Nova Scotia, interpreted as an inlier of Grenvillian basement (Miller and Barr, 2000). Paleozoic igneous activity within the inlier is demonstrated by the 435 +7/−3 Ma Sammys Barren granite (Miller and others, 1996) and other units interpreted to be Paleozoic in age, including the Fox Back Ridge granodiorite, smaller gabbroic plutons, and mafic and felsic dikes (Miller, ms, 1997) which may be the feeders to volcanic rocks observed in the Acadian foreland basin. We interpret that the Blair River Inlier is a likely source

terrane for the Red Island Road Formation as it explains both the prevalence of Grenvillian zircon and Silurian felsic volcanic cobbles.

All foreland basin successions in western Newfoundland demonstrate Laurentian affinity (fig. 3R) despite the fact that Gondwanan terranes were accreted to the composite Laurentian margin during both the Salinic and Acadian orogenies. A possible explanation for the lack of Gondwanan detritus within the basin is that all Gondwanan terranes were accreted to the Laurentian margin on the lower plate (Waldron and others, 2012), and underthrust beneath Laurentia. It is likely that this material was topographically lower than the orogen to the west, and Gondwanan detritus was only incorporated into basins developed on top or to the east of the orogen.

CONCLUSIONS

New detrital zircon geochronology results from the foreland basin successions in western Newfoundland indicate that the post-Taconic successions are not derived from the same source region as the earlier Middle Ordovician Goose Tickle Group. Our interpretation of previously published U/Pb analyses of zircon indicates that the Goose Tickle Group was derived from clastic units within the Humber Arm Allochthon. We interpret a major shift in provenance during deposition of the Long Point Group (fig. 2), indicated by a decrease in the relative abundance of 1.85 Ga zircon accompanied by a reversal in dominant unidirectional paleoflow indicators from SW to NE (Quinn, ms, 1992; Batten Hender and Dix, 2008). The dominant 1.1 Ga Grenville peaks within spectra of the Long Point Group and Clam Bank Formation are similar to age spectra presented in detrital zircon studies of rift and passive margin clastics in the Québec and New England Appalachians (fig. 3). We suggest that the Long Point Group was sourced from either the Québec or New England portion of the orogen. Another major shift in provenance occurs during deposition of the Early Devonian Red Island Road Formation. An overwhelming abundance of 1.1 Ga zircon and a minor proportion of older Mesoproterozoic zircon indicate derivation from a similar source region to that which provided detritus to the oldest rift-related sediments – basement units of the Grenville Orogen. In addition to an entirely Grenvillian derived sandstone units, there are abundant rhyolite cobbles one of which is dated at 421 Ma – with no known local source. Although the La Poile Group may be a source candidate for the rhyolite cobbles, the combination of U/Pb age data for detrital zircon and lithologic observations lead us to suggest that the Grenville Blair River Inlier in Cape Breton, which has a palinspastically restored position east of the basin during the Devonian, is also a possible source terrane for the Red Island Road detritus. Basement massifs were uplifted along deep-seated basement faults during Acadian orogenesis and detritus from these massifs likely filled Acadian foreland basins.

ACKNOWLEDGMENTS

Work in western Newfoundland was supported by Petroleum Exploration Enhancement Program, a joint initiative of both the Newfoundland and Labrador Provincial Government and Nalcor Energy, which provided funding for this research. JWFW's contribution was supported by Natural Sciences and Engineering Resesarch Council Discovery Grant. We thank Ian Atkinson at Nalcor and Wes Foote at the Newfoundland Department of Natural Resources for their support. Tiffany Miller and Morgan Snyder assisted in the field. Christy Rowe and Nicholas Harris provided useful comments and discussions on the thesis that formed the basis for this paper. We are grateful to journal reviewers Alexei Zagorevski and Francis Macdonald, and to Associate Editor Robert Wintsch for their helpful comments and suggestions, which substantially improved the paper.

APPENDIX
METHODS: U/Pb GEOCHRONOLOGY

Detrital Zircon Geochronlogy

Sample preparation.—All samples were crushed and then sieved through a 250 μm sieve. Light minerals were then removed using a Wilfley table.

The remaining heavy separates were then bathed in 10% acetic acid to remove carbonate material (except NP021A as it did not contain carbonate) and then all samples were bathed in 3% hydrogen peroxide to clean clays from the material. After washing, samples were placed in sodium polytungstate ($\rho = 2.8$) for further heavy mineral extraction before processing using the Frantz Isodynamic and Barrier separators (for example, Rosenblum and Brownfield, 2000) to remove magnetic minerals. Finally, the remaining heavy separates were placed in diiodomethane (MI) to extract the final heavy mineral separate that contained zircon.

To ensure an unbiased sample, zircon grains were not individually picked. We placed all grains from the heavy separates in a tray and removed obvious material that was not zircon. All remaining grains were then mounted on epoxy. In order to expose sections in the grains, the mounts were polished using 1200 μm sandpaper and then by using 0.3 μm Al oxide powder on a Pellon polishing cloth. Grains were imaged using scanning electron microscope techniques in both secondary electron and cathodeluminescence imaging using the scanning electron microscope in the Canadian Center for Isotope Microanalysis (CCIM) facility at the University of Alberta.

Analysis.—The analyses were carried out in the ICPMS facility at the University of Alberta, using the Nu Plasma multicollector inductively coupled plasma mass spectrometer (MC-ICP-MS), interfaced with a NewWave UP-213 laser ablation system. Procedures were modified from Simonetti et al. (2005). A laser beam diameter of 30 μm was used and, because of the small size of most grains, only a single analysis was carried out per zircon. We used zircon images to avoid straddling any obvious core-rim boundaries during analyses. The zircon grains were analysed in groups of 10 to 15, separated by analysis of in-house standards: LH94-15 (1830 ± 1 Ma; Ashton and others, 1999; Simonetti and others, 2005) and GJ1-32 (608 Ma; Jackson and others, 2004; Elhlou and others, 2006). The total number of sample grains analyzed ranged from 111 to 137. In cases where counts at mass 204 were significantly elevated (> 450 counts per second), a common-Pb correction was applied using the two stage evolution model (Stacey and Kramers, 1975) to estimate the common-Pb isotopic composition.

Data reduction.—All analytical results are reported in the Appendix. Data were reduced using an Excel-based spreadsheet in which isotopic ratios were normalized to the standard analyses. For grains with uncorrected $^{207}Pb/^{206}Pb$ ratios less than 0.0658 (corresponding to an age of 800 Ma) we normalize using in-house standard GJ1-32 (608 Ma; Jackson and others, 2004) and report the $^{206}Pb/^{238}U$ age which is typically more precise for younger grains. For grains with uncorrected $^{207}Pb/^{206}Pb$ greater than 0.0658 (800 Ma) we normalize to in- house standard LH94-15 (1.83 Ga; Ashton and others, 1999) and report $^{207}Pb/^{206}Pb$ age. All errors are expressed as 2σ and are a quadratic combination of the standard deviation of the standard means and standard error of the measured isotopic ratio. Only grains which were> 90 % concordant were used in our calculations and interpretations.

Data reduction.—The software Isoplot (Ludwig, 2012) was used to produce probability density functions (PDF) (fig. 3) for all samples analysed in this study. Concordia diagrams (fig. 6), weighted means, mean square of weighted deviates (MSWD) calculations, and other statistical analyses were prepared with the same software. Cumulative density functions and Kolmogorov-Smirnov (K-S) critical values (fig. 7) were calculated using software from the Arizona LaserChron Center (Gehrels and others, 2006).

The PDF, the most common tool used when comparing zircon age distributions, is the sum of the probability distributions derived from individual grains and their analytical errors, which compares the probability of finding zircon of different ages within the sample. The function displays this information in an intuitive fashion (fig. 3) so that we subjectively identify similar age peaks, gaps in data, and differences in peak height as a method of comparing and contrasting the data sets.

Detrital zircon data collected by others and used in this study are re-plotted as PDFs in order draw comparisons with our results (fig. 3). We use our chosen cutoff age (800 Ma) when plotting the $^{206}Pb/^{207}Pb$ versus $^{206}Pb/^{238}U$ age for others' data. We also exclude analyses which are discordant by >10%. These adjustments account for minor differences between the re-plotted PDFs (fig. 3) and previously published plots.

In addition to PDFs, we also use the Kolmogorov-Smirnoff (K-S) test as a means of mathematically comparing distributions in order to determine if there is a statistically significant difference between the distributions. This method, based on the cumulative density functions (CDF), tests the null hypothesis that the two samples are derived from the same parent population. If the maximum difference in probability between two curves (D) is greater than a critical value (dependent on the number of analyses), the null hypothesis is rejected. Ibanez-Mejia (2018) has expressed caution in the use of the K-S test, using results from modern river sediments to deduce that hydrodynamic factors can introduce statistically significant differences in zircon distributions even in sediment samples from the same source area. However, populations of zircon from ancient marine sandstones show much greater homogeneity than those from modern rivers, suggesting that more effective mixing occurs in marine environments. A recent review of methods by

Vermeesch (2018) concludes that the K-S test is one of the more effective quantitative tools available for comparing detrital zircon populations.

TIMS ananlysis.—A rhyolite boulder from a conglomeratic bed within the Red Island Road Formation (NP 021E) was collected for U-Pb dating of zircon using Chemical Abrasion Thermal Ionization Mass Spectrometry (CA-TIMS). Preparation and analyses were carried out at Memorial University of Newfoundland. The boulder was washed and scrubbed to remove any debris, then processed with standard techniques of crushing and concentration of a heavy mineral separate and then zircon separation. Zircon crystals were examined under the microscope and the clearest, sharpest euhedral prisms were selected for analysis (fig. 5E). The zircon grains are high quality small euhedral prisms and inclusions, of likely apatite and/or melt, are visible as well as clear hematite staining along fractures (fig. 5E).

All grains were chemically abraded using the Mattinson (2005) chemical abrasion thermal ion mass spectrometry (CA-TIMS) technique. Selected grains were annealed 36 hours in an oven at 1000 °C, then etched in concentrated hydrofluoric acid in a Teflon capsule at 200 °C in an oven for 4 hours. This procedure is designed to remove any altered domains in the crystal that may have undergone Pb loss. Pb and U isotopic ratios were measured by thermal ionization mass spectrometry, and results calculated using Isoplot (Ludwig, 2012). Further details of the lab procedures are presented in Sparkes and Dunning (2014).

TABLE A1

Data for NP007 Lourdes Formation

	Isotopic ratios										Apparent age summary						
sample name	^{206}Pb (cps)	^{204}Pb (cps)	$\frac{^{207}Pb}{^{206}Pb}$	2σ	$\frac{^{207}Pb}{^{235}U}$	2σ	$\frac{^{206}Pb}{^{238}U}$	2σ	r	Com Pb corrected	age (Ma) $\frac{^{207}Pb^*}{^{206}Pb^*}$	error (Ma) 2σ	age (Ma) $\frac{^{207}Pb^*}{^{235}U}$	error (Ma) 2σ	age (Ma) $\frac{^{206}Pb^*}{^{238}U}$	error (Ma) 2σ	disc. %
Better than ± 10% discordant																	
NP007-100	75601	206	0.07128	0.00083	1.50576	0.11675	0.15322	0.01175	0.989	no	965	24	933	46	919	65	5.1
NP007-093	266284	210	0.07128	0.00075	1.54015	0.11533	0.15670	0.01162	0.990	no	966	21	947	45	938	64	3.0
NP007-086	108036	201	0.07253	0.00079	1.65213	0.06878	0.16520	0.00664	0.965	no	1001	22	990	26	986	37	1.6
NP007-130	38613	175	0.07281	0.00086	1.60352	0.08603	0.15972	0.00836	0.976	no	1009	24	972	33	955	46	5.7
NP007-021	219977	244	0.07324	0.00084	1.67431	0.07151	0.16581	0.00682	0.963	no	1021	23	999	27	989	38	3.3
NO007-013	182951	174	0.07346	0.00080	1.70463	0.06767	0.16829	0.00642	0.961	no	1027	22	1010	25	1003	35	2.5
NP007-090	71413	220	0.07349	0.00090	1.69384	0.07294	0.16717	0.00690	0.959	no	1027	25	1006	27	996	38	3.3
NO007-073	126755	0	0.07359	0.00080	1.62240	0.07305	0.15989	0.00699	0.970	no	1030	22	979	28	956	39	7.7
NP007-088	124677	279	0.07369	0.00081	1.70886	0.08008	0.16820	0.00766	0.972	no	1033	22	1012	30	1002	42	3.2
NP007-102	246952	197	0.07373	0.00078	1.66759	0.08179	0.16404	0.00786	0.977	no	1034	21	996	31	979	43	5.7
NP007-025	137052	321	0.07379	0.00080	1.66832	0.06764	0.16397	0.00641	0.964	no	1036	22	997	25	979	35	5.9
NP007-110	138966	259	0.07387	0.00081	1.62306	0.06069	0.15935	0.00570	0.956	no	1038	22	979	23	953	32	8.8
NP007-049	111694	225	0.07399	0.00084	1.73969	0.09531	0.17054	0.00914	0.978	no	1041	23	1023	35	1015	50	2.7
NP007-036	64642	410	0.07409	0.00086	1.61426	0.06890	0.15802	0.00649	0.962	no	1044	23	976	26	946	36	10.1
NP007-055	102499	8	0.07421	0.00087	1.69092	0.06735	0.16526	0.00629	0.956	no	1047	23	1005	25	986	35	6.3
NO007-076	108989	0	0.07452	0.00087	1.66434	0.07108	0.16198	0.00665	0.961	no	1056	23	995	27	968	37	9.0
NP007-071	156752	0	0.07458	0.00087	1.66981	0.06806	0.16239	0.00634	0.958	no	1057	23	997	26	970	35	8.9
NP007-007	59093	13	0.07484	0.00094	1.70123	0.09761	0.16487	0.00923	0.976	no	1064	25	1009	36	984	51	8.1
NP007-085	680207	242	0.07487	0.00078	1.78663	0.09148	0.17306	0.00867	0.979	no	1065	21	1041	33	1029	47	3.7
NP007-124	90914	303	0.07507	0.00094	1.79782	0.10365	0.17370	0.00978	0.976	no	1070	25	1045	37	1032	53	3.8
NP007-024	949402	428	0.07509	0.00076	1.85468	0.08557	0.17915	0.00806	0.975	no	1071	20	1065	30	1062	44	0.9
NP007-059	151443	62	0.07511	0.00083	1.79241	0.06993	0.17307	0.00648	0.959	no	1072	22	1043	25	1029	36	4.3
NP007-064	91917	86	0.07527	0.00082	1.81064	0.07183	0.17447	0.00665	0.961	no	1076	22	1049	26	1037	36	3.9
NP007-030	151340	345	0.07536	0.00083	1.78164	0.06893	0.17146	0.00636	0.958	no	1078	22	1039	25	1020	35	5.8
NP007-048	203115	164	0.07539	0.00079	1.85139	0.11663	0.17811	0.01106	0.986	no	1079	21	1064	41	1057	60	2.2
NP007-062	90545	19	0.07580	0.00084	1.83234	0.08206	0.17532	0.00761	0.969	no	1090	22	1057	29	1041	42	4.8
NP007-051	85868	189	0.07587	0.00091	1.80932	0.10394	0.17296	0.00972	0.978	no	1092	24	1049	37	1028	53	6.3
NP007-005	159355	118	0.07589	0.00111	1.75969	0.13117	0.16818	0.01229	0.980	no	1092	29	1031	47	1002	67	8.9
NP007-029	59792	284	0.07627	0.00101	1.84853	0.07784	0.17578	0.00703	0.950	no	1102	26	1063	27	1044	38	5.7
NO007-011	98024	320	0.07635	0.00093	1.83491	0.07411	0.17430	0.00671	0.954	no	1104	24	1058	26	1036	37	6.7
NP007-065	59105	73	0.07651	0.00089	1.80982	0.07180	0.17156	0.00651	0.956	no	1108	23	1049	26	1021	36	8.6
NP007-058	76897	207	0.07672	0.00096	1.81463	0.06870	0.17154	0.00613	0.944	no	1114	25	1051	24	1021	34	9.1
NP007-070	72297	0	0.07696	0.00096	1.84778	0.07463	0.17414	0.00669	0.951	no	1120	25	1063	26	1035	37	8.2
NP007-114	237180	262	0.07738	0.00084	1.97373	0.21007	0.18499	0.01959	0.995	no	1131	21	1107	69	1094	106	3.5
NP007-068	113352	2	0.07742	0.00087	1.88845	0.08371	0.17691	0.00759	0.967	no	1132	22	1077	29	1050	41	7.9
NO007-016	111562	277	0.07748	0.00086	1.94329	0.07943	0.18191	0.00715	0.962	no	1134	22	1096	27	1077	39	5.4
NP007-094	198031	468	0.07767	0.00082	1.96982	0.14719	0.18395	0.01361	0.990	no	1138	21	1105	49	1088	74	4.8
NO007-018	94531	26	0.07925	0.00093	2.04131	0.09415	0.18681	0.00833	0.967	no	1178	23	1129	31	1104	45	6.9
NP007-035	251474	388	0.07931	0.00087	1.99295	0.09098	0.18226	0.00808	0.971	no	1180	22	1113	30	1079	44	9.3
NO007-014	783420	171	0.07935	0.00084	1.98865	0.07895	0.18176	0.00695	0.964	no	1181	21	1112	26	1077	38	9.6
NP007-057	57078	132	0.07993	0.00101	2.13145	0.09177	0.19339	0.00796	0.956	no	1195	25	1159	29	1140	43	5.1

TABLE A1
(continued)

sample name	^{206}Pb (cps)	^{204}Pb (cps)	Isotopic ratios $\frac{^{207}Pb}{^{206}Pb}$	2σ	$\frac{^{207}Pb}{^{235}U}$	2σ	$\frac{^{206}Pb}{^{238}U}$	2σ	r	Com Pb corrected	Apparent age summary age (Ma) $\frac{^{207}Pb^*}{^{206}Pb^*}$	error (Ma) 2σ	age (Ma) $\frac{^{207}Pb^*}{^{235}U}$	error (Ma) 2σ	age (Ma) $\frac{^{206}Pb^*}{^{238}U}$	error (Ma) 2σ	disc. %
Better than ± 10% discordant																	
NO007-019	241422	138	0.08040	0.00099	2.09425	0.08016	0.18892	0.00685	0.947	no	1207	24	1147	26	1116	37	8.2
NP007-045	314137	78	0.08077	0.00086	2.21216	0.12799	0.19865	0.01129	0.983	no	1216	21	1185	40	1168	60	4.3
NP007-113	73175	229	0.08107	0.00094	2.09599	0.22897	0.18751	0.02037	0.994	no	1223	23	1147	72	1108	110	10.2
NP007-097	115992	401	0.08118	0.00088	2.13718	0.15720	0.19094	0.01389	0.989	no	1226	21	1161	50	1126	75	8.8
NO007-020	170976	65	0.08173	0.00089	2.31442	0.08908	0.20538	0.00758	0.959	no	1239	21	1217	27	1204	40	3.1
NP007-039	45016	175	0.08293	0.00113	2.26569	0.10405	0.19815	0.00869	0.955	no	1268	26	1202	32	1165	47	8.8
NP007-061	272427	124	0.08517	0.00110	2.44381	0.09069	0.20810	0.00724	0.938	no	1319	25	1256	26	1219	39	8.4
NP007-112	29436	221	0.08562	0.00116	2.47036	0.26562	0.20926	0.02232	0.992	no	1330	26	1263	75	1225	118	8.6
NP007-127	233119	116	0.08569	0.00092	2.62087	0.14405	0.22183	0.01196	0.981	no	1331	21	1307	40	1292	63	3.3
NP007-120	135011	204	0.08688	0.00093	2.62781	0.27859	0.21938	0.02314	0.995	no	1358	20	1308	75	1279	121	6.4
NP007-099	384569	319	0.08825	0.00092	2.60316	0.19397	0.21394	0.01579	0.990	no	1388	20	1302	53	1250	83	10.9
NP007-128	206527	148	0.08899	0.00099	2.85287	0.15371	0.23252	0.01226	0.979	no	1404	21	1370	40	1348	64	4.4
NP007-082	117808	469	0.08976	0.00096	2.88092	0.13187	0.23278	0.01036	0.972	no	1420	20	1377	34	1349	54	5.6
NP007-060	41361	48	0.09128	0.00131	2.95602	0.12344	0.23486	0.00921	0.939	no	1453	27	1396	31	1360	48	7.1
NP007-009	117003	0	0.09169	0.00106	2.98300	0.18100	0.23595	0.01405	0.982	no	1461	22	1403	45	1366	73	7.2
NP007-119	484633	399	0.09264	0.00095	3.11533	0.32747	0.24390	0.02551	0.995	no	1481	19	1436	78	1407	131	5.5
NO007-015	93842	305	0.09779	0.00117	3.47663	0.13942	0.25785	0.00987	0.955	no	1582	22	1522	31	1479	50	7.3
NP007-095	84165	338	0.10034	0.00117	3.63804	0.30173	0.26295	0.02159	0.990	no	1630	21	1558	64	1505	109	8.6
NP007-038	284102	277	0.10112	0.00105	3.90849	0.14842	0.28034	0.01024	0.962	no	1645	19	1615	30	1593	51	3.5
NP007-032	85021	337	0.10150	0.00111	3.81809	0.18358	0.27283	0.01277	0.974	no	1652	20	1597	38	1555	64	6.6
NP007-091A	223812	297	0.10159	0.00118	3.78926	0.16021	0.27052	0.01100	0.961	no	1653	21	1590	33	1543	56	7.5
NO007-075	215385	26	0.10224	0.00112	3.89035	0.17237	0.27598	0.01185	0.969	no	1665	20	1612	35	1571	60	6.4
NO007-012	93850	258	0.10225	0.00118	3.83435	0.15298	0.27197	0.01039	0.957	no	1665	21	1600	32	1551	52	7.7
NP007-083	169283	665	0.10641	0.00112	4.29362	0.19975	0.29264	0.01326	0.974	no	1739	19	1692	38	1655	66	5.5
NP007-108	69369	203	0.11456	0.00129	4.76395	0.19175	0.30161	0.01166	0.960	no	1873	20	1779	33	1699	57	10.5
NO007-079	114510	0	0.11562	0.00123	5.07683	0.19819	0.31845	0.01196	0.962	no	1890	19	1832	33	1782	58	6.5
NP007-089	817955	333	0.11682	0.00119	5.08287	0.25400	0.31556	0.01544	0.979	no	1908	18	1833	42	1768	75	8.4
NP007-037	216725	291	0.17109	0.00174	10.79527	0.48275	0.45761	0.01993	0.974	no	2568	17	2506	41	2429	88	6.5
NO007-081	43847	1	0.17129	0.00191	11.26701	0.54672	0.47707	0.02253	0.973	no	2570	19	2545	44	2514	98	2.6
NP007-053	201402	78	0.17733	0.00191	11.74797	0.64880	0.48049	0.02603	0.981	no	2628	18	2585	50	2529	112	4.5
NP007-105	395541	205	0.17859	0.00188	11.59477	0.49202	0.47086	0.01936	0.969	no	2640	17	2572	39	2487	84	7.0
NP007-056	515812	75	0.17965	0.00187	11.13819	0.42872	0.44966	0.01666	0.963	no	2650	17	2535	35	2394	74	11.5
NP007-006	655480	30	0.18421	0.00205	12.54935	0.72803	0.49409	0.02813	0.981	no	2691	18	2646	53	2588	120	4.6
NP007-035	251474	388	0.07931	0.00087	1.99295	0.09098	0.18226	0.00808	0.971	no	1180	22	1113	30	1079	44	9.3
NO007-078	100839	1	0.18446	0.00192	12.45122	0.50730	0.48957	0.01928	0.967	no	2693	17	2639	38	2569	83	5.6
NP007-001	325006	0	0.18517	0.00210	12.55261	0.72971	0.49165	0.02803	0.981	no	2700	19	2647	53	2578	120	5.5
NP007-040	301756	166	0.18654	0.00190	13.16839	0.43311	0.51200	0.01601	0.951	no	2712	17	2692	31	2665	68	2.1
NP007-028	722669	264	0.18679	0.00195	13.01344	0.51206	0.50529	0.01917	0.964	no	2714	17	2681	36	2636	82	3.5
NP007-044	725511	126	0.18706	0.00191	12.97349	0.73909	0.50301	0.02819	0.984	no	2716	17	2678	52	2627	120	4.0

TABLE A1
(continued)

sample name	^{206}Pb (cps)	^{204}Pb (cps)	Isotopic ratios $\frac{^{207}Pb}{^{206}Pb}$	2σ	$\frac{^{207}Pb}{^{235}U}$	2σ	$\frac{^{206}Pb}{^{238}U}$	2σ	r	Com Pb corrected	Apparent age summary age (Ma) $\frac{^{207}Pb^*}{^{206}Pb^*}$	error (Ma) 2σ	age (Ma) $\frac{^{207}Pb^*}{^{235}U}$	error (Ma) 2σ	age (Ma) $\frac{^{206}Pb^*}{^{238}U}$	error (Ma) 2σ	disc. %
Better than ± 10% discordant																	
NP007-116	666447	173	0.18717	0.00193	13.01260	1.37956	0.50423	0.05320	0.995	no	2717	17	2681	95	2632	224	3.8
NP007-121	184384	215	0.18738	0.00191	12.48669	1.31745	0.48330	0.05075	0.995	no	2719	17	2642	95	2542	217	7.9
NP007-022	169575	270	0.18920	0.00199	13.41246	0.57832	0.51413	0.02150	0.970	no	2735	17	2709	40	2674	91	2.7
NP007-023	691631	232	0.19890	0.00203	14.68409	0.56808	0.53543	0.01998	0.965	no	2817	17	2795	36	2764	83	2.3
NP007-046	458600	118	0.20265	0.00221	14.29719	0.86443	0.51169	0.03043	0.984	no	2848	18	2770	56	2664	128	7.9
NP007-054	135523	26	0.20336	0.00236	15.09937	0.65568	0.53851	0.02254	0.964	no	2853	19	2822	41	2777	94	3.3
NP007-043	548024	182	0.20457	0.00211	15.42873	0.87388	0.54699	0.03046	0.983	no	2863	17	2842	53	2813	126	2.2
NP007-042	97691	149	0.20461	0.00210	15.78749	0.87861	0.55960	0.03061	0.983	no	2863	17	2864	52	2865	125	-0.1
Discordance >10% or <-10%																	
NP007-092	39036	214	0.07450	0.00102	1.62609	0.12280	0.15831	0.01176	0.984	no	1055	27	980	46	947	65	11.0
NP007-087	31275	188	0.07518	0.00111	1.66723	0.06802	0.16084	0.00612	0.932	no	1073	29	996	26	961	34	11.2
NP007-098	747358	430	0.11107	0.00114	4.38737	0.33258	0.28648	0.02152	0.991	no	1817	19	1710	61	1624	107	12.0
NP007-103	534594	299	0.11317	0.00119	4.53717	0.18645	0.29077	0.01155	0.967	no	1851	19	1738	34	1645	57	12.6
NP007-115	139961	290	0.08557	0.00115	2.36995	0.26539	0.20087	0.02233	0.993	no	1329	26	1234	77	1180	119	12.2
NP007-067	42643	3	0.07672	0.00101	1.75495	0.06748	0.16590	0.00599	0.940	no	1114	26	1029	25	989	33	12.1
NO007-080	903121	43	0.11030	0.00115	4.27165	0.16621	0.28088	0.01053	0.963	no	1804	19	1688	32	1596	53	13.0
NP007-002	53053	255	0.07753	0.00102	1.79199	0.11268	0.16764	0.01031	0.978	no	1135	26	1043	40	999	57	12.9
NO007-017	73323	183	0.05774	0.00087	0.58189	0.03659	0.07309	0.00446	0.971	no	520	33	466	23	455	27	13.0
NP007-107	36157	229	0.07710	0.00141	1.74493	0.07250	0.16413	0.00612	0.897	no	1124	36	1025	26	980	34	13.8
NP007-003	80244	116	0.07300	0.00099	1.47652	0.08920	0.14670	0.00864	0.975	no	1014	27	921	36	882	48	13.9
NP007-118	124658	150	0.05764	0.00069	0.57324	0.02532	0.07212	0.00307	0.963	no	516	26	460	16	449	18	13.5
NP007-066	45905	12	0.08132	0.00142	2.02104	0.08155	0.18025	0.00656	0.902	no	1229	34	1123	27	1068	36	14.2
NP007-126	475453	214	0.18678	0.00200	11.29400	0.67348	0.43855	0.02573	0.984	no	2714	18	2548	54	2344	114	16.2
NP007-026	493482	358	0.10497	0.00112	3.72440	0.23740	0.25732	0.01617	0.986	no	1714	20	1577	50	1476	82	15.5
NP007-101	321587	291	0.08233	0.00090	2.06843	0.15159	0.18220	0.01321	0.989	no	1253	21	1138	49	1079	72	15.1
NP007-050	79314	186	0.09051	0.00105	2.61225	0.20114	0.20931	0.01593	0.988	no	1436	22	1304	55	1225	84	16.1
NP007-010	29593	0	0.07934	0.00128	1.84727	0.11744	0.16887	0.01039	0.967	no	1181	31	1062	41	1006	57	16.0
NP007-008	49608	13	0.07777	0.00132	1.73732	0.11047	0.16202	0.00993	0.964	no	1141	33	1022	40	968	55	16.3
NP007-123	128435	491	0.08270	0.00166	2.05532	0.11279	0.18025	0.00921	0.931	no	1262	39	1134	37	1068	50	16.7
NP007-092	39036	214	0.07450	0.00102	1.62609	0.12280	0.15831	0.01176	0.984	no	1055	27	980	46	947	65	11.0
NP007-087	31275	188	0.07518	0.00111	1.66723	0.06802	0.16084	0.00612	0.932	no	1073	29	996	26	961	34	11.2
NP007-098	747358	430	0.11107	0.00114	4.38737	0.33258	0.28648	0.02152	0.991	no	1817	19	1710	61	1624	107	12.0
NP007-103	534594	299	0.11317	0.00119	4.53717	0.18645	0.29077	0.01155	0.967	no	1851	19	1738	34	1645	57	12.6
NP007-115	139961	290	0.08557	0.00115	2.36995	0.26539	0.20087	0.02233	0.993	no	1329	26	1234	77	1180	119	12.2
NP007-067	42643	3	0.07672	0.00101	1.75495	0.06748	0.16590	0.00599	0.940	no	1114	26	1029	25	989	33	12.1
NO007-080	903121	43	0.11030	0.00115	4.27165	0.16621	0.28088	0.01053	0.963	no	1804	19	1688	32	1596	53	13.0
NP007-002	53053	255	0.07753	0.00102	1.79199	0.11268	0.16764	0.01031	0.978	no	1135	26	1043	40	999	57	12.9
NO007-017	73323	183	0.05774	0.00087	0.58189	0.03659	0.07309	0.00446	0.971	no	520	33	466	23	455	27	13.0
NP007-107	36157	229	0.07710	0.00141	1.74493	0.07250	0.16413	0.00612	0.897	no	1124	36	1025	26	980	34	13.8

TABLE A1
(continued)

sample name	Isotopic ratios									Apparent age summary							
	^{206}Pb (cps)	^{204}Pb (cps)	$\frac{^{207}Pb}{^{206}Pb}$	2σ	$\frac{^{207}Pb}{^{235}U}$	2σ	$\frac{^{206}Pb}{^{238}U}$	2σ	r	Com Pb corrected	age (Ma) $\frac{^{207}Pb^*}{^{206}Pb^*}$	error (Ma) 2σ	age (Ma) $\frac{^{207}Pb^*}{^{235}U}$	error (Ma) 2σ	age (Ma) $\frac{^{206}Pb^*}{^{238}U}$	error (Ma) 2σ	disc. %
Discordance >10% or <-10%																	
NP007-003	80244	116	0.07300	0.00099	1.47652	0.08920	0.14670	0.00864	0.975	no	1014	27	921	36	882	48	13.9
NP007-118	124658	150	0.05764	0.00069	0.57324	0.02532	0.07212	0.00307	0.963	no	516	26	460	16	449	18	13.5
NP007-066	45905	12	0.08132	0.00142	2.02104	0.08155	0.18025	0.00656	0.902	no	1229	34	1123	27	1068	36	14.2
NP007-126	475453	214	0.18678	0.00200	11.29400	0.67348	0.43855	0.02573	0.984	no	2714	18	2548	54	2344	114	16.2
NP007-026	493482	358	0.10497	0.00112	3.72440	0.23740	0.25732	0.01617	0.986	no	1714	20	1577	50	1476	82	15.5
NP007-101	321587	291	0.08233	0.00090	2.06843	0.15159	0.18220	0.01321	0.989	no	1253	21	1138	49	1079	72	15.1
NP007-050	79314	186	0.09051	0.00105	2.61225	0.20114	0.20931	0.01593	0.988	no	1436	22	1304	55	1225	84	16.1
NP007-010	29593	0	0.07934	0.00128	1.84727	0.11744	0.16887	0.01039	0.967	no	1181	31	1062	41	1006	57	16.0
NP007-008	49608	13	0.07777	0.00132	1.73732	0.11047	0.16202	0.00993	0.964	no	1141	33	1022	40	968	55	16.3
NP007-123	128435	491	0.08270	0.00166	2.05532	0.11279	0.18025	0.00921	0.931	no	1262	39	1134	37	1068	50	16.7
NP007-125	37552	203	0.07725	0.00135	1.68589	0.09852	.00135	0.00883	0.954	no	1128	34	1003	37	947	49	17.2
NP007-004	630166	226	0.07799	0.00090	1.69228	0.10655	0.00090	0.00974	0.983	no	1147	23	1006	39	942	54	19.2
NP007-033	20852	453	0.08102	0.00175	1.85790	0.08286	0.00175	0.00650	0.876	no	1222	42	1066	29	992	36	20.3
NP007-047	36154	204	0.07942	0.00227	1.75515	0.11039	0.00227	0.00898	0.891	no	1183	55	1029	40	958	50	20.4
NP007-027	342666	337	0.10802	0.00115	3.62783	0.13207	0.00115	0.00848	0.957	no	1766	19	1556	29	1405	44	22.7
NP007-084	296239	484	0.07894	0.00109	1.68172	0.07653	0.00109	0.00670	0.953	no	1171	27	1002	29	926	37	22.4
NP007-122	758497	303	0.18989	0.00206	10.30158	0.54765	0.00206	0.02048	0.979	no	2741	18	2462	48	2139	94	25.8
NP007-106	20294	206	0.08302	0.00172	1.88864	0.08128	0.00172	0.00622	0.876	no	1270	40	1077	28	984	34	24.2
NO007-077	10285	0	0.08526	0.00186	1.98595	0.09382	0.00186	0.00708	0.888	no	1321	42	1111	31	1006	39	25.7
NP007-129	1388295	219	0.10033	0.00109	2.77019	0.14273	0.00109	0.01009	0.977	no	1630	20	1348	38	1177	54	30.4
NP007-109	231313	459	0.09942	0.00102	2.70393	0.13649	0.00102	0.00975	0.979	no	1613	19	1330	37	1161	52	30.6
NP007-069	367719	102	0.07971	0.00093	1.55858	0.10042	0.00093	0.00899	0.983	no	1190	23	954	39	855	51	30.0
NP007-096	205712	204	0.11781	0.00177	3.67733	0.31983	0.00177	0.01939	0.985	no	1923	27	1566	67	1316	101	34.9
NP007-034	7904	247	0.08919	0.00198	1.94748	0.10347	0.00198	0.00765	0.909	no	1408	42	1098	35	948	42	35.1
NO007-072	491312	205	0.20820	0.00219	9.50435	0.53342	0.00219	0.01825	0.982	no	2892	17	2388	50	1844	88	41.5
NP007-052	932757	558	0.16463	0.00186	6.03043	0.30309	0.00186	0.01301	0.974	no	2504	19	1980	43	1519	66	44.0
NP007-104	607575	455	0.16264	0.00234	5.75194	0.37455	0.00234	0.01629	0.975	no	2483	24	1939	55	1472	83	45.4
NP007-031	47188	299	0.06869	0.00312	0.68435	0.03967	0.00312	0.00261	0.622	no	889	91	529	24	450	16	51.2
NP007-111	512834	279	0.18372	0.00224	4.54790	0.26550	0.00224	0.01025	0.978	no	2687	20	1740	47	1064	56	65.3

TABLE A2

Data for NG024A Winterhouse Formation

			Isotopic ratios								Apparent age summary						
sample name	^{206}Pb (cps)	^{204}Pb (cps)	$\frac{^{207}Pb}{^{206}Pb}$	2σ	$\frac{^{207}Pb}{^{235}U}$	2σ	$\frac{^{206}Pb}{^{238}U}$	2σ	r	Com Pb corrected	age (Ma) $\frac{^{207}Pb^*}{^{206}Pb^*}$	error (Ma) 2σ	age (Ma) $\frac{^{207}Pb^*}{^{235}U}$	error (Ma) 2σ	age (Ma) $\frac{^{206}Pb^*}{^{238}U}$	error (Ma) 2σ	disc. %
Better than ± 10% discordant																	
NGO24A-120	51289	40	0.05633	0.00075	0.54031	0.02011	0.06957	0.00242	0.934	no	465	29	439	13	434	15	7.0
NGO24A-043	139248	175	0.05700	0.00063	0.59591	0.03729	0.07582	0.00467	0.984	no	492	24	475	23	471	28	4.3
NG024A-005	146030	0	0.07068	0.00133	1.52555	0.06144	0.15655	0.00557	0.884	no	948	38	941	24	938	31	1.2
NG024A-26	112575	33	0.07205	0.00079	1.55194	0.05629	0.15621	0.00540	0.953	no	987	22	951	22	936	30	5.6
NG024A-066	36782	113	0.07351	0.00102	1.56597	0.13363	0.15451	0.01301	0.987	no	1028	28	957	52	926	72	10.6
NG024-098	290183	88	0.07232	0.00075	1.58262	0.05610	0.15872	0.00538	0.956	no	995	21	963	22	950	30	4.9
NG024-104	103893	23	0.07288	0.00080	1.62386	0.06412	0.16161	0.00613	0.961	no	1010	22	979	25	966	34	4.8
NG024A-059	155882	175	0.07416	0.00080	1.65148	0.13557	0.16151	0.01314	0.991	no	1046	22	990	51	965	73	8.3
NG024A-067	119262	126	0.07410	0.00087	1.67060	0.13828	0.16351	0.01340	0.990	no	1044	24	997	51	976	74	7.0
NG024A-074	131163	215	0.07305	0.00079	1.68477	0.13932	0.16726	0.01371	0.992	no	1015	22	1003	51	997	75	2.0
NG024A-094	122518	249	0.07362	0.00079	1.71236	0.06110	0.16869	0.00574	0.954	no	1031	21	1013	23	1005	32	2.7
NG024A-058	54010	258	0.07501	0.00095	1.71833	0.14349	0.16614	0.01371	0.988	no	1069	25	1015	52	991	75	7.9
NG024A-009	139202	0	0.07302	0.00136	1.75937	0.06905	0.17475	0.00604	0.880	no	1014	37	1031	25	1038	33	-2.5
NGO24A-113	217270	34	0.07402	0.00078	1.76326	0.06874	0.17278	0.00649	0.963	no	1042	21	1032	25	1027	36	1.5
NGO24A-122	162128	77	0.07505	0.00104	1.76874	0.06558	0.17093	0.00588	0.928	no	1070	28	1034	24	1017	32	5.3
NGO24A-042	90240	185	0.07551	0.00090	1.76994	0.08117	0.16999	0.00753	0.966	no	1082	24	1034	29	1012	41	7.0
NGO24-108	43407	33	0.07598	0.00112	1.77803	0.07561	0.16972	0.00677	0.938	no	1095	29	1037	27	1011	37	8.3
NG024A-075	337488	253	0.07392	0.00078	1.78922	0.13261	0.17555	0.01288	0.990	no	1039	21	1042	47	1043	70	-0.4
NG024A-084	73963	179	0.07586	0.00088	1.79271	0.13489	0.17139	0.01274	0.988	no	1091	23	1043	48	1020	70	7.1
NGO24A-119	125401	41	0.07484	0.00082	1.79447	0.06752	0.17390	0.00626	0.957	no	1064	22	1043	24	1034	34	3.1
NG024A-079	147073	163	0.07603	0.00087	1.79748	0.13191	0.17147	0.01243	0.988	no	1096	23	1045	47	1020	68	7.5
NGO24A-048	68905	235	0.07587	0.00106	1.80763	0.08244	0.17279	0.00750	0.952	no	1092	28	1048	29	1027	41	6.4
NGO24A-006	51386	0	0.07401	0.00147	1.82192	0.08006	0.17854	0.00700	0.892	no	1042	40	1053	28	1059	38	-1.8
NG024A-091	44543	280	0.07670	0.00090	1.83298	0.13498	0.17332	0.01260	0.987	no	1113	23	1057	47	1030	69	8.1
NG024A-28	82112	51	0.07618	0.00084	1.83809	0.06327	0.17499	0.00570	0.947	no	1100	22	1059	22	1040	31	5.9
NGO24A-124	298833	76	0.07570	0.00083	1.83984	0.06800	0.17627	0.00622	0.955	no	1087	22	1060	24	1047	34	4.0
NG024A-065	92739	126	0.07543	0.00089	1.84132	0.15124	0.17706	0.01439	0.990	no	1080	24	1060	53	1051	78	2.9
NGO24A-054	99996	289	0.07636	0.00091	1.88519	0.08674	0.17905	0.00796	0.966	no	1105	24	1076	30	1062	43	4.2
NG024A-020	55422	111	0.07704	0.00086	1.88520	0.06951	0.17747	0.00624	0.953	no	1122	22	1076	24	1053	34	6.7
NG024A-23	51454	34	0.07703	0.00099	1.89496	0.06888	0.17841	0.00606	0.935	no	1122	25	1079	24	1058	33	6.2
NG024A-27	264720	51	0.07593	0.00081	1.91822	0.06766	0.18323	0.00616	0.953	no	1093	21	1087	23	1085	33	0.8
NG024A-080	289981	208	0.07813	0.00096	1.92278	0.14994	0.17848	0.01374	0.988	no	1150	24	1089	51	1059	75	8.6
NG024A-004	31698	0	0.07714	0.00199	1.92537	0.07817	0.18102	0.00567	0.772	no	1125	51	1090	27	1073	31	5.1
NG024-110	123109	42	0.07543	0.00085	1.93427	0.08893	0.18598	0.00829	0.970	no	1080	22	1093	30	1100	45	-2.0
NG024A-014	123942	114	0.07825	0.00110	1.93565	0.07485	0.17942	0.00647	0.932	no	1153	28	1093	26	1064	35	8.4
NGO24A-116	178984	34	0.07678	0.00082	1.93896	0.07317	0.18315	0.00663	0.959	no	1116	21	1095	25	1084	36	3.1
NGO24A-114	83476	29	0.07657	0.00095	1.94250	0.07696	0.18400	0.00693	0.950	no	1110	24	1096	26	1089	38	2.1
NG024A-089	350800	219	0.07776	0.00080	1.95838	0.15724	0.18267	0.01455	0.992	no	1141	20	1101	53	1082	79	5.6
NG024A-032	68755	20	0.07706	0.00095	1.96187	0.10137	0.18465	0.00926	0.971	no	1123	24	1103	34	1092	50	2.9
NGO24A-052	43490	305	0.07847	0.00121	2.03299	0.09515	0.18790	0.00830	0.944	no	1159	30	1127	31	1110	45	4.6
NG024A-037	285029	62	0.07839	0.00085	2.07800	0.09863	0.19226	0.00888	0.973	no	1157	21	1142	32	1134	48	2.2

TABLE A2
(continued)

sample name	^{206}Pb (cps)	^{204}Pb (cps)	Isotopic ratios $\frac{^{207}Pb}{^{206}Pb}$	2σ	$\frac{^{207}Pb}{^{235}U}$	2σ	$\frac{^{206}Pb}{^{238}U}$	2σ	r	Com Pb corrected	Apparent age summary age (Ma) $\frac{^{207}Pb^*}{^{206}Pb^*}$	error (Ma) 2σ	age (Ma) $\frac{^{207}Pb^*}{^{235}U}$	error (Ma) 2σ	age (Ma) $\frac{^{206}Pb^*}{^{238}U}$	error (Ma) 2σ	disc. %
Better than ± 10% discordant																	
NG024-097A	121129	86	0.08101	0.00093	2.10197	0.07574	0.18818	0.00642	0.947	no	1222	22	1149	24	1112	35	9.8
NGO24A-044	27385	158	0.08282	0.00115	2.22784	0.10705	0.19509	0.00897	0.957	no	1265	27	1190	33	1149	48	10.0
NG024A-038	42553	56	0.08529	0.00204	2.40847	0.16265	0.20479	0.01293	0.935	no	1322	46	1245	47	1201	69	10.0
NG024A-29	58014	38	0.08352	0.00111	2.44653	0.08934	0.21244	0.00723	0.932	no	1281	26	1256	26	1242	38	3.4
NG024A-073	111526	215	0.08540	0.00090	2.51897	0.21448	0.21392	0.01807	0.992	no	1325	20	1278	60	1250	95	6.2
NG024A-086	256049	270	0.08926	0.00095	2.81730	0.20894	0.22891	0.01680	0.990	no	1410	20	1360	54	1329	88	6.4
NGO24A-123	67172	70	0.08851	0.00106	2.82262	0.11020	0.23128	0.00859	0.951	no	1394	23	1362	29	1341	45	4.2
NGO24A-115	297200	21	0.08672	0.00096	2.84160	0.12172	0.23765	0.00983	0.966	no	1354	21	1367	32	1374	51	-1.6
NG024A-013	68885	92	0.09118	0.00108	3.06128	0.11013	0.24350	0.00827	0.944	no	1450	22	1423	27	1405	43	3.5
NG024A-21	96586	74	0.09172	0.00103	3.14405	0.11005	0.24861	0.00824	0.947	no	1462	21	1444	27	1431	42	2.3
NG024A-21	96586	74	0.09172	0.00103	3.14405	0.11005	0.24861	0.00824	0.947	no	1462	21	1444	27	1431	42	2.3
NG024A-035	442091	32	0.09142	0.00095	3.16536	0.14803	0.25111	0.01145	0.975	no	1455	20	1449	35	1444	59	0.9
NG024A-22	123595	64	0.09172	0.00115	3.18682	0.11109	0.25198	0.00819	0.933	no	1462	24	1454	27	1449	42	1.0
NGO24A-117	220322	32	0.09311	0.00099	3.19974	0.12112	0.24925	0.00906	0.960	no	1490	20	1457	29	1435	47	4.2
NGO24A-051	99335	298	0.09269	0.00109	3.26478	0.14780	0.25545	0.01117	0.966	no	1482	22	1473	35	1467	57	1.1
NG024A-093	180974	273	0.09436	0.00102	3.26941	0.24100	0.25129	0.01832	0.989	no	1515	20	1474	56	1445	94	5.2
NG024A-070	335500	104	0.09524	0.00099	3.28506	0.26945	0.25016	0.02035	0.992	no	1533	20	1478	62	1439	104	6.8
NGO24A-047	308224	207	0.09149	0.00095	3.29557	0.14881	0.26125	0.01148	0.973	no	1457	20	1480	35	1496	58	-3.0
NGO24A-045	308605	221	0.09286	0.00101	3.31791	0.14722	0.25914	0.01115	0.970	no	1485	20	1485	34	1485	57	0.0
NGO24A-072	110622	207	0.09624	0.00111	3.40670	0.28761	0.25673	0.02147	0.991	no	1552	21	1506	64	1473	109	5.7
NG024A-036	445648	53	0.09399	0.00098	3.40981	0.16355	0.26312	0.01232	0.976	no	1508	20	1507	37	1506	63	0.2
NGO24A-041	514918	124	0.09419	0.00098	3.45354	0.16637	0.26592	0.01251	0.976	no	1512	19	1517	37	1520	63	-0.6
NG024A-30	524101	159	0.09670	0.00129	3.56141	0.17239	0.26711	0.01243	0.961	no	1561	25	1541	38	1526	63	2.5
NG024A-088	310289	205	0.10063	0.00106	3.65026	0.26660	0.26308	0.01901	0.990	no	1636	19	1561	57	1506	96	8.9
NG024A-068	76986	142	0.10321	0.00118	3.95548	0.32866	0.27795	0.02288	0.991	no	1683	21	1625	65	1581	114	6.8
NGO24A-111	310498	33	0.10095	0.00106	4.04487	0.14783	0.29060	0.01017	0.958	no	1642	19	1643	29	1645	51	-0.2
NG024A-033	292373	17	0.10272	0.00108	4.14467	0.20486	0.29265	0.01413	0.977	no	1674	19	1663	40	1655	70	1.3
NGO24A-050	414475	251	0.10201	0.00103	4.16760	0.18715	0.29632	0.01296	0.974	no	1661	19	1668	36	1673	64	-0.8
NG024A-019	202614	135	0.10330	0.00111	4.18410	0.14591	0.29376	0.00975	0.951	no	1684	20	1671	28	1660	48	1.6
NG024-099	150712	92	0.10575	0.00114	4.20867	0.14523	0.28863	0.00946	0.950	no	1727	20	1676	28	1635	47	6.1
NG024A-25	2434822	91	0.10177	0.00104	4.28343	0.14475	0.30525	0.00984	0.953	no	1657	19	1690	27	1717	48	-4.2
NG024A-010	212753	962	0.11163	0.00668	4.55619	0.31832	0.29602	0.01067	0.516	yes	1826	105	1741	57	1672	53	9.6
NG024-107	51385	41	0.10712	0.00145	4.55837	0.23866	0.30862	0.01561	0.966	no	1751	25	1742	43	1734	76	1.1
NG024A-008	1360386	78	0.10766	0.00201	4.61698	0.19147	0.31102	0.01151	0.893	no	1760	34	1752	34	1746	56	0.9
NG024A-017	321547	163	0.11011	0.00118	4.82105	0.17826	0.31755	0.01124	0.957	no	1801	19	1789	31	1778	55	1.5
NG024A-087	401069	271	0.11352	0.00124	4.84766	0.36304	0.30970	0.02294	0.989	no	1857	20	1793	61	1739	112	7.2
NG024-103	106936	30	0.11236	0.00118	4.91221	0.17302	0.31707	0.01066	0.954	no	1838	19	1804	29	1775	52	3.9
NG024A-034	305630	73	0.11249	0.00117	4.96051	0.23763	0.31984	0.01495	0.976	no	1840	19	1813	40	1789	73	3.2
NG024A-011	428062	148	0.11131	0.00118	5.05710	0.16529	0.32952	0.01019	0.946	no	1821	19	1829	27	1836	49	-1.0
NG024A-001	580471	0	0.11050	0.00204	5.16746	0.19457	0.33918	0.01113	0.872	no	1808	33	1847	32	1883	53	-4.8
NG024A-012	407139	132	0.11394	0.00118	5.31942	0.18833	0.33860	0.01147	0.957	no	1863	19	1872	30	1880	55	-1.0

TABLE A2
(continued)

sample name	^{206}Pb (cps)	^{204}Pb (cps)	Isotopic ratios $\frac{^{207}Pb}{^{206}Pb}$	2σ	$\frac{^{207}Pb}{^{235}U}$	2σ	$\frac{^{206}Pb}{^{238}U}$	2σ	r	Com Pb corrected	Apparent age summary age (Ma) $\frac{^{207}Pb^*}{^{206}Pb^*}$	error (Ma) 2σ	age (Ma) $\frac{^{207}Pb^*}{^{235}U}$	error (Ma) 2σ	age (Ma) $\frac{^{206}Pb^*}{^{238}U}$	error (Ma) 2σ	disc. %
Better than ± 10% discordant																	
NGO24A-118	473759	95	0.11784	0.00120	5.37071	0.18475	0.33056	0.01086	0.955	no	1924	18	1880	29	1841	52	4.9
NG024A-040	279118	56	0.11688	0.00126	5.46660	0.26402	0.33921	0.01597	0.975	no	1909	19	1895	41	1883	76	1.6
NG024A-064	641741	173	0.16293	0.00187	9.53130	0.78787	0.42428	0.03473	0.990	no	2486	19	2391	73	2280	155	9.8
NG024A-031	569121	14	0.16369	0.00166	10.46746	0.49760	0.46380	0.02154	0.977	no	2494	17	2477	43	2456	94	1.8
NG024A-007	84572	0	0.18477	0.00358	12.94360	0.49784	0.50807	0.01688	0.864	no	2696	32	2676	36	2648	72	2.2
NG024-106	637337	59	0.18856	0.00192	13.03664	0.48527	0.50144	0.01796	0.962	no	2730	17	2682	35	2620	77	4.9
NGO24A-055	226990	258	0.19078	0.00195	13.43827	1.09870	0.51088	0.04144	0.992	no	2749	17	2711	74	2660	174	3.9
NGO24A-049	166891	247	0.18555	0.00192	13.63566	0.59759	0.53299	0.02270	0.972	no	2703	17	2725	41	2754	95	-2.3
NG024A-057	84284	270	0.19135	0.00202	13.69437	1.15530	0.51905	0.04344	0.992	no	2754	17	2729	77	2695	182	2.6
NG024A-083	358735	179	0.19436	0.00207	13.77726	1.02286	0.51411	0.03777	0.990	no	2779	17	2735	68	2674	159	4.6
NG024A-081	95204	248	0.19914	0.00273	13.95444	1.04857	0.50822	0.03755	0.983	no	2819	22	2747	69	2649	159	7.4
NG024A-002	173510	0	0.18951	0.00349	14.32000	0.51854	0.54803	0.01708	0.861	no	2738	30	2771	34	2817	71	-3.6
NG024-109	251008	43	0.20285	0.00210	15.23789	0.54229	0.54482	0.01855	0.957	no	2849	17	2830	33	2804	77	2.0
NG024A-24	226799	54	0.25375	0.00261	22.44843	0.79631	0.64163	0.02178	0.957	no	3208	16	3203	34	3195	85	0.5
NG024-100	171861	78	0.33439	0.00362	33.94395	1.29007	0.73622	0.02682	0.959	no	3637	16	3608	37	3557	99	2.9
Discordance >10% or <-10%																	
NGO24A-112	64947	60	0.08123	0.00120	2.09240	0.07792	0.18682	0.00638	0.918	no	1227	29	1146	25	1104	35	10.9
NG024A-085	37099	206	0.08079	0.00103	2.05734	0.15155	0.18469	0.01340	0.985	no	1216	25	1135	49	1093	72	11.1
NGO24A-053	40448	307	0.07495	0.00107	1.65671	0.07878	0.16031	0.00727	0.954	no	1067	28	992	30	958	40	11.0
NG024-096	98161	151	0.07472	0.00096	1.63943	0.06415	0.15913	0.00588	0.945	no	1061	26	985	24	952	33	11.1
NG024A-090	172301	335	0.09857	0.00189	3.37793	0.25357	0.24856	0.01804	0.967	no	1597	35	1499	57	1431	92	11.6
NG024A-095	61728	249	0.07815	0.00099	1.85386	0.13758	0.17205	0.01258	0.985	no	1151	25	1065	48	1023	69	12.0
NG024A-062	659095	227	0.18609	0.00216	11.57016	0.96398	0.45094	0.03720	0.990	no	2708	19	2570	75	2399	163	13.6
NG024A-076	36720	164	0.07429	0.00096	1.58692	0.12036	0.15492	0.01158	0.985	no	1049	26	965	46	928	64	12.4
NG024A-078	30830	153	0.07746	0.00113	1.79140	0.13519	0.16772	0.01242	0.981	no	1133	29	1042	48	1000	68	12.7
NG024A-039	61370	46	0.07620	0.00120	1.69932	0.08383	0.16174	0.00756	0.948	no	1100	31	1008	31	966	42	13.1
NG024A-56	211954	331	0.08020	0.00136	1.96471	0.16376	0.17768	0.01450	0.979	no	1202	33	1103	55	1054	79	13.3
NG024A-060	81934	187	0.05702	0.00073	0.53598	0.03683	0.06817	0.00460	0.983	no	492	28	436	24	425	28	14.1
NG024-105	163904	162	0.11054	0.00157	4.16369	0.17952	0.27318	0.01112	0.944	no	1808	26	1667	35	1557	56	15.6
NG024A-069	20799	124	0.07636	0.00125	1.64153	0.14066	0.15591	0.01311	0.981	no	1105	32	986	53	934	73	16.6
NG024A-061	125625	191	0.05813	0.00069	0.57978	0.03928	0.07234	0.00482	0.984	no	534	26	464	25	450	29	16.3
NG024A-082	53216	209	0.08434	0.00208	2.12594	0.16608	0.18283	0.01355	0.949	no	1300	47	1157	53	1082	73	18.2
NG024-102	377553	183	0.08039	0.00164	1.76196	0.08022	0.15896	0.00647	0.894	no	1207	40	1032	29	951	36	22.8
NG024A-063	80437	161	0.05935	0.00070	0.59013	0.04058	0.07211	0.00488	0.985	no	580	26	471	26	449	29	23.4
NG024A-092	49702	319	0.08135	0.00143	1.77269	0.14087	0.15803	0.01225	0.975	no	1230	34	1036	50	946	68	24.8
NG024A-071	11757	190	0.08782	0.00170	2.13150	0.18707	0.17603	0.01507	0.975	no	1379	37	1159	59	1045	82	26.2
NG024A-015	446167	160	0.10403	0.00106	3.15486	0.13065	0.21995	0.00883	0.969	no	1697	19	1446	31	1282	46	27.0
NG024-101	78163	65	0.06138	0.00078	0.64601	0.02773	0.07633	0.00313	0.955	no	653	27	506	17	474	19	28.4
NGO24A-121	103537	75	0.06082	0.00076	0.58895	0.02224	0.07023	0.00250	0.944	no	633	27	470	14	438	15	31.9

TABLE A2
(continued)

sample name	^{206}Pb (cps)	^{204}Pb (cps)	Isotopic ratios $\frac{^{207}Pb}{^{206}Pb}$	2σ	$\frac{^{207}Pb}{^{235}U}$	2σ	$\frac{^{206}Pb}{^{238}U}$	2σ	r	Com Pb corrected	Apparent age summary age (Ma) $\frac{^{207}Pb^*}{^{206}Pb^*}$	error (Ma) 2σ	age (Ma) $\frac{^{207}Pb^*}{^{235}U}$	error (Ma) 2σ	age (Ma) $\frac{^{206}Pb^*}{^{238}U}$	error (Ma) 2σ	disc. %
Discordance >10% or <-10%																	
NG024A-003	320941	2528	0.09259	0.00907	2.18829	0.22592	0.17141	0.00559	0.316	yes	1480	175	1177	70	1020	31	33.6
NGO24A-125	51861	227	0.11750	0.00168	2.88041	0.12232	0.17779	0.00711	0.941	no	1919	25	1377	32	1055	39	48.7
NG024A-077	43588	191	0.06462	0.00133	0.57779	0.04390	0.06485	0.00474	0.963	no	762	43	463	28	405	29	48.3
NG024A-016	30556	93	0.06628	0.00198	0.62689	0.02779	0.06860	0.00225	0.740	no	815	61	494	17	428	14	49.1
NGO24A-046	219984	428	0.07165	0.00073	0.53598	0.03683	0.06817	0.00460	0.983	no	976	33	565	20	468	20	53.9

TABLE A3

Data for NG043 Clam Bank Formation

			Isotopic ratios								Apparent age summary						
sample name	^{206}Pb (cps)	^{204}Pb (cps)	$\frac{^{207}Pb}{^{206}Pb}$	2σ	$\frac{^{207}Pb}{^{235}U}$	2σ	$\frac{^{206}Pb}{^{238}U}$	2σ	r	Com Pb corrected	age (Ma) $\frac{^{207}Pb^*}{^{206}Pb^*}$	error (Ma) 2σ	age (Ma) $\frac{^{207}Pb^*}{^{235}U}$	error (Ma) 2σ	age (Ma) $\frac{^{206}Pb^*}{^{238}U}$	error (Ma) 2σ	disc. %
Better than ± 10% discordant																	
NG043-074	234163	7	0.05631	0.00061	0.52847	0.01874	0.06807	0.00230	0.953	no	465	24	431	12	425	14	8.9
NG043-013	211962	0	0.05694	0.00068	0.58655	0.02399	0.07471	0.00292	0.956	no	489	26	469	15	464	18	5.2
NG043-015	98885	0	0.07254	0.00109	1.61569	0.06877	0.16154	0.00643	0.936	no	1001	30	976	26	965	36	3.9
NG043-133	433644	19	0.07270	0.00084	1.59139	0.06720	0.15877	0.00645	0.962	no	1005	23	967	26	950	36	5.9
NG043-031	2659920	2567	0.07330	0.00125	1.68872	0.07222	0.16708	0.00655	0.917	yes	1022	34	1004	27	996	36	2.8
NG043-107	544858	1	0.07413	0.00077	1.83233	0.07678	0.17926	0.00727	0.968	no	1045	21	1057	27	1063	40	-1.8
NG043-111	79028	0	0.07459	0.00130	1.69968	0.08115	0.16527	0.00735	0.931	no	1057	35	1008	30	986	41	7.3
NG043-060	373982	0	0.07465	0.00079	1.83093	0.07876	0.17789	0.00742	0.969	no	1059	21	1057	28	1055	40	0.4
NG043-120	1081866	3	0.07472	0.00078	1.91003	0.07766	0.18541	0.00729	0.967	no	1061	21	1085	27	1096	40	-3.6
NG043-127	263033	63	0.07478	0.00080	1.83114	0.07320	0.17760	0.00684	0.964	no	1063	21	1057	26	1054	37	0.9
NG043-124	455832	33	0.07494	0.00108	1.81675	0.10234	0.17583	0.00957	0.966	no	1067	29	1052	36	1044	52	2.3
NG043-052	142612	11	0.07495	0.00081	1.89273	0.07310	0.18315	0.00679	0.960	no	1067	22	1079	25	1084	37	-1.7
NG043-068	191411	0	0.07514	0.00086	1.84773	0.08004	0.17835	0.00745	0.964	no	1072	23	1063	28	1058	41	1.4
NG043-102	309343	2	0.07520	0.00080	1.89746	0.07884	0.18301	0.00735	0.967	no	1074	21	1080	27	1083	40	-1.0
NG043-079	205563	7	0.07530	0.00104	1.75902	0.07178	0.16943	0.00650	0.941	no	1077	28	1030	26	1009	36	6.8
NG043-003	281333	0	0.07555	0.00079	1.94627	0.09445	0.18685	0.00885	0.976	no	1083	21	1097	32	1104	48	-2.1
NG043-007	211793	47	0.07556	0.00082	1.92762	0.10000	0.18501	0.00939	0.978	no	1084	22	1091	34	1094	51	-1.1
NG043-131	425494	1	0.07559	0.00080	1.85283	0.08404	0.17777	0.00784	0.973	no	1084	21	1064	29	1055	43	3.0
NG043-123	151125	0	0.07575	0.00096	1.84374	0.07830	0.17652	0.00715	0.954	no	1089	25	1061	28	1048	39	4.0
NG043-104	63594	7	0.07580	0.00135	1.73066	0.07334	0.16558	0.00637	0.908	no	1090	35	1020	27	988	35	10.1
NG043-033	161313	103	0.07583	0.00099	1.80895	0.07493	0.17302	0.00680	0.949	no	1091	26	1049	27	1029	37	6.1
NG043-055	68955	4	0.07598	0.00097	1.84492	0.07342	0.17611	0.00663	0.947	no	1095	25	1062	26	1046	36	4.8
NG043-117	152208	0	0.07616	0.00111	1.79388	0.07157	0.17084	0.00635	0.931	no	1099	29	1043	26	1017	35	8.1
NG043-113	357892	0	0.07653	0.00079	2.00780	0.09016	0.19027	0.00831	0.973	no	1109	21	1118	30	1123	45	-1.4
NG043-029	71450	3	0.07673	0.00263	1.88733	0.09431	0.17839	0.00648	0.727	no	1114	67	1077	33	1058	35	5.5
NG043-010	164944	24	0.07688	0.00101	1.90171	0.09544	0.17939	0.00869	0.965	no	1118	26	1082	33	1064	47	5.3
NG043-037	180366	1336	0.07733	0.00960	1.83565	0.23810	0.17217	0.00645	0.289	yes	1130	229	1058	82	1024	35	10.1
NG043-134	141676	0	0.07749	0.00104	1.95891	0.08653	0.18335	0.00772	0.953	no	1134	27	1102	29	1085	42	4.7
NG043-072	188794	15	0.07756	0.00147	1.87636	0.07673	0.17546	0.00636	0.886	no	1136	37	1073	27	1042	35	8.9
NG043-039	252031	111	0.07764	0.00101	1.85212	0.07447	0.17301	0.00659	0.947	no	1138	26	1064	26	1029	36	10.4
NG043-022	250780	6	0.07766	0.00099	1.98374	0.08793	0.18526	0.00786	0.958	no	1138	25	1110	29	1096	43	4.1
NG043-005	47855	0	0.07772	0.00113	1.90417	0.09258	0.17770	0.00824	0.954	no	1140	29	1083	32	1054	45	8.1
NG043-040	218467	195	0.07792	0.00087	1.96671	0.08284	0.18305	0.00744	0.965	no	1145	22	1104	28	1084	40	5.8
NG043-047	56926	162	0.07803	0.00121	1.92030	0.08499	0.17848	0.00740	0.937	no	1148	30	1088	29	1059	40	8.4
NG043-038	965030	119	0.07846	0.00087	2.19206	0.08183	0.20263	0.00722	0.955	no	1159	22	1179	26	1189	39	-2.9
NG043-126	84285	7	0.07873	0.00122	1.98106	0.07541	0.18250	0.00634	0.913	no	1165	30	1109	25	1081	34	7.9
NG043-090	66343	2	0.07908	0.00163	1.95551	0.10104	0.17935	0.00850	0.917	no	1174	40	1100	34	1063	46	10.2
NG043-121	209915	25	0.07935	0.00117	2.06255	0.08462	0.18852	0.00722	0.933	no	1181	29	1136	28	1113	39	6.2
NG043-018	22117	36	0.07941	0.00346	2.02550	0.13516	0.18500	0.00935	0.757	no	1182	84	1124	44	1094	51	8.1
NG043-014	458927	46	0.07984	0.00203	2.06858	0.09388	0.18791	0.00706	0.828	no	1193	49	1138	31	1110	38	7.6
NG043-034	351605	258	0.07985	0.00148	2.02586	0.08093	0.18401	0.00651	0.885	no	1193	36	1124	27	1089	35	9.5

TABLE A3
(continued)

sample name	Isotopic ratios										Apparent age summary						
	^{206}Pb (cps)	^{204}Pb (cps)	$\frac{^{207}Pb}{^{206}Pb}$	2σ	$\frac{^{207}Pb}{^{235}U}$	2σ	$\frac{^{206}Pb}{^{238}U}$	2σ	r	Com Pb corrected	age (Ma) $\frac{^{207}Pb^*}{^{206}Pb^*}$	error (Ma) 2σ	age (Ma) $\frac{^{207}Pb^*}{^{235}U}$	error (Ma) 2σ	age (Ma) $\frac{^{206}Pb^*}{^{238}U}$	error (Ma) 2σ	disc. %
Better than ± 10% discordant																	
NG043-044	101833	151	0.08011	0.00197	2.03715	0.09224	0.18443	0.00700	0.839	no	1200	48	1128	30	1091	38	9.8
NG043-008	207446	0	0.08019	0.00121	2.16717	0.10588	0.19600	0.00910	0.951	no	1202	30	1171	33	1154	49	4.4
NG043-110	205186	43	0.08075	0.00098	2.29157	0.10045	0.20583	0.00867	0.961	no	1215	24	1210	31	1207	46	0.8
NG043-051	83227	17	0.08139	0.00104	2.26020	0.09362	0.20141	0.00793	0.951	no	1231	25	1200	29	1183	42	4.3
NG043-058	70711	0	0.08157	0.00125	2.17410	0.09684	0.19331	0.00808	0.938	no	1235	30	1173	31	1139	44	8.5
NG043-046	54253	171	0.08158	0.00149	2.30393	0.12075	0.20483	0.01006	0.937	no	1235	35	1213	36	1201	54	3.0
NG043-069	1020449	6	0.08319	0.00086	2.50504	0.09747	0.21840	0.00819	0.964	no	1274	20	1273	28	1273	43	0.0
NG043-089	457500	1	0.08390	0.00088	2.61178	0.12267	0.22578	0.01034	0.975	no	1290	20	1304	34	1312	54	-1.9
NG043-023	578151	0	0.08612	0.00089	2.87522	0.11477	0.24213	0.00934	0.966	no	1341	20	1375	30	1398	48	-4.7
NG043-050	383282	74	0.08798	0.00093	3.06044	0.11171	0.25230	0.00881	0.957	no	1382	20	1423	28	1450	45	-5.5
NG043-057	407030	3	0.08867	0.00099	3.01843	0.11518	0.24690	0.00901	0.956	no	1397	21	1412	29	1422	46	-2.0
NG043-080	241251	51	0.08931	0.00138	2.93290	0.12772	0.23816	0.00970	0.935	no	1411	29	1390	32	1377	50	2.7
NG043-030	778055	1	0.08949	0.00097	3.11868	0.12145	0.25274	0.00945	0.960	no	1415	21	1437	30	1453	48	-3.0
NG043-109	291971	1	0.08983	0.00101	3.02299	0.12735	0.24407	0.00991	0.964	no	1422	21	1413	32	1408	51	1.1
NG043-035	346421	164	0.09056	0.00126	2.92392	0.12428	0.23418	0.00940	0.945	no	1437	26	1388	32	1356	49	6.2
NG043-053	391905	20	0.09327	0.00122	3.33200	0.13279	0.25910	0.00976	0.945	no	1493	24	1489	31	1485	50	0.6
NG043-026	643992	3	0.09371	0.00097	3.34425	0.12185	0.25882	0.00904	0.959	no	1502	19	1491	28	1484	46	1.4
NG043-088	353272	4	0.09452	0.00097	3.48118	0.13441	0.26713	0.00994	0.964	no	1518	19	1523	30	1526	50	-0.6
NG043-082	319778	7	0.09455	0.00098	3.46184	0.15191	0.26556	0.01132	0.971	no	1519	20	1519	34	1518	57	0.1
NG043-002	309386	0	0.09484	0.00097	3.48349	0.16780	0.26640	0.01254	0.977	no	1525	19	1523	37	1523	64	0.2
NG043-125	683881	620	0.09492	0.00188	3.32990	0.16132	0.25444	0.01125	0.913	yes	1526	37	1488	37	1461	58	4.8
NG043-004	129890	0	0.09509	0.00114	3.58932	0.19532	0.27376	0.01453	0.975	no	1530	22	1547	42	1560	73	-2.2
NG043-083	147098	0	0.09521	0.00104	3.39139	0.14011	0.25835	0.01030	0.965	no	1532	20	1502	32	1481	53	3.7
NG043-077	1454764	972	0.09536	0.00145	3.38022	0.12477	0.25708	0.00865	0.911	yes	1535	28	1500	29	1475	44	4.4
NG043-129	236596	16	0.09554	0.00100	3.41401	0.15855	0.25918	0.01172	0.974	no	1539	20	1508	36	1486	60	3.9
NG043-048	644900	2124	0.09611	0.00358	3.50454	0.17349	0.26445	0.00862	0.658	yes	1550	68	1528	38	1513	44	2.7
NG043-081	373474	410	0.09761	0.00247	3.41909	0.16970	0.25406	0.01085	0.861	yes	1579	47	1509	38	1459	56	8.5
NG043-115	680642	59	0.09810	0.00116	3.80637	0.16852	0.28141	0.01201	0.964	no	1588	22	1594	35	1598	60	-0.7
NG043-049	1325621	10239	0.09885	0.00752	3.55290	0.31701	0.26068	0.01217	0.523	yes	1603	136	1539	68	1493	62	7.6
NG043-084	250231	1	0.09886	0.00109	3.57487	0.15904	0.26227	0.01130	0.969	no	1603	21	1544	35	1501	57	7.1
NG043-070	418642	11	0.09997	0.00109	3.54458	0.13333	0.25715	0.00926	0.957	no	1624	20	1537	29	1475	47	10.2
NG043-132	266994	35	0.10038	0.00155	3.92497	0.15645	0.28358	0.01042	0.922	no	1631	28	1619	32	1609	52	1.5
NG043-017	465644	2	0.10108	0.00135	4.07411	0.16999	0.29233	0.01156	0.948	no	1644	25	1649	33	1653	57	-0.6
NG043-001	163964	0	0.10203	0.00109	4.13479	0.19903	0.29392	0.01379	0.975	no	1661	20	1661	39	1661	68	0.0
NG043-119	438872	131	0.10321	0.00117	4.42135	0.20071	0.31069	0.01365	0.968	no	1683	21	1716	37	1744	67	-4.2
NG043-041	711574	334	0.10326	0.00106	3.93105	0.20012	0.27611	0.01377	0.979	no	1683	19	1620	40	1572	69	7.5
NG043-114	345375	39	0.10408	0.00129	4.20018	0.16568	0.29267	0.01096	0.949	no	1698	23	1674	32	1655	54	2.9
NG043-130	213768	19	0.10510	0.00137	4.34711	0.17982	0.29998	0.01177	0.949	no	1716	24	1702	34	1691	58	1.6
NG043-116	1139775	0	0.10694	0.00108	4.63768	0.17794	0.31452	0.01164	0.965	no	1748	18	1756	32	1763	57	-1.0
NG043-054	499191	18	0.10763	0.00114	4.65698	0.18859	0.31381	0.01227	0.965	no	1760	19	1760	33	1759	60	0.0
NG043-135	565632	24	0.10932	0.00142	4.82463	0.20943	0.32009	0.01326	0.954	no	1788	23	1789	36	1790	64	-0.1

TABLE A3
(continued)

sample name	^{206}Pb (cps)	^{204}Pb (cps)	Isotopic ratios $\frac{^{207}Pb}{^{206}Pb}$	2σ	$\frac{^{207}Pb}{^{235}U}$	2σ	$\frac{^{206}Pb}{^{238}U}$	2σ	r	Com Pb corrected	Apparent age summary age (Ma) $\frac{^{207}Pb^*}{^{206}Pb^*}$	error (Ma) 2σ	age (Ma) $\frac{^{207}Pb^*}{^{235}U}$	error (Ma) 2σ	age (Ma) $\frac{^{206}Pb^*}{^{238}U}$	error (Ma) 2σ	disc. %
Better than ± 10% discordant																	
NG043-099	377629	1	0.10934	0.00120	4.80988	0.19234	0.31904	0.01226	0.961	no	1788	20	1787	33	1785	60	0.2
NG043-066	226554	0	0.11037	0.00116	4.80381	0.20006	0.31567	0.01272	0.967	no	1806	19	1786	34	1769	62	2.3
NG043-078	1349339	2	0.11097	0.00121	5.16380	0.21817	0.33751	0.01378	0.966	no	1815	20	1847	35	1875	66	-3.8
NG043-019	526626	18	0.11283	0.00138	5.58640	0.29171	0.35908	0.01823	0.972	no	1846	22	1914	44	1978	86	-8.3
NG043-016	1194307	11	0.11592	0.00136	5.65097	0.24289	0.35357	0.01462	0.962	no	1894	21	1924	36	1952	69	-3.5
NG043-101	367933	1517	0.11903	0.00475	5.42511	0.30837	0.33056	0.01337	0.712	yes	1942	70	1889	48	1841	64	6.0
NG043-028	209457	0	0.12348	0.00131	6.39160	0.24075	0.37543	0.01357	0.959	no	2007	19	2031	33	2055	63	-2.8
NG043-061	235171	0	0.17374	0.00179	12.11442	0.46892	0.50571	0.01886	0.964	no	2594	17	2613	36	2638	80	-2.1
NG043-076	573937	10	0.17949	0.00198	12.69895	0.51091	0.51314	0.01985	0.961	no	2648	18	2658	37	2670	84	-1.0
NG043-059	1880810	74	0.18551	0.00188	13.27439	0.55307	0.51898	0.02097	0.970	no	2703	17	2699	39	2695	88	0.4
NG043-042	937591	301	0.18721	0.00206	13.80503	0.53465	0.53483	0.01986	0.959	no	2718	18	2736	36	2762	83	-2.0
NG043-045	560368	210	0.18755	0.00204	13.88241	0.58542	0.53684	0.02188	0.966	no	2721	18	2742	39	2770	91	-2.2
NG043-100	328250	1	0.19290	0.00206	14.83748	0.54307	0.55786	0.01953	0.956	no	2767	17	2805	34	2858	80	-4.1
NG043-012	946229	123	0.19517	0.00238	14.47527	0.59981	0.53791	0.02130	0.956	no	2786	20	2781	39	2775	89	0.5
NG043-112	405049	1022	0.20018	0.00407	15.09813	0.66350	0.54703	0.02132	0.887	yes	2828	33	2821	41	2813	88	0.6
NG043-106	342759	9	0.22016	0.00227	17.81924	0.71868	0.58700	0.02289	0.967	no	2982	16	2980	38	2977	92	0.2
Discordance >10% or <-10%																	
NG043-071	73295	7	0.07367	0.00114	1.57256	0.07817	0.15481	0.00731	0.950	no	1033	31	959	30	928	41	10.9
NG043-025	87723	0	0.09274	0.00194	2.92789	0.14901	0.22899	0.01063	0.912	no	1482	39	1389	38	1329	55	11.4
NG043-020	483808	1	0.07687	0.00121	1.76597	0.10483	0.16663	0.00954	0.964	no	1118	31	1033	38	994	52	12.0
NG043-097	26908	0	0.07563	0.00153	1.68225	0.06710	0.16132	0.00554	0.861	no	1085	40	1002	25	964	31	12.0
NG043-105	93128	90	0.07912	0.00161	1.91237	0.09319	0.17531	0.00777	0.909	no	1175	40	1085	32	1041	42	12.3
NG043-086	69368	34	0.08023	0.00332	1.97621	0.13354	0.17864	0.00954	0.790	no	1203	80	1107	45	1060	52	12.9
NG043-073	309012	94	0.10756	0.00258	4.01666	0.21558	0.27085	0.01300	0.894	no	1758	43	1638	43	1545	66	13.6
NG043-103	154094	19	0.07775	0.00123	1.80145	0.07154	0.16805	0.00612	0.917	no	1140	31	1046	26	1001	34	13.2
NG043-094	126100	41	0.07939	0.00303	1.89888	0.12422	0.17347	0.00921	0.812	no	1182	74	1081	43	1031	50	13.8
NG043-021	227722	20	0.07806	0.00247	1.80868	0.09216	0.16805	0.00670	0.783	no	1148	62	1049	33	1001	37	13.8
NG043-009	157979	0	0.09180	0.00196	2.76890	0.20174	0.21877	0.01524	0.956	no	1463	40	1347	53	1275	80	14.1
NG043-092	405640	595	0.11444	0.00280	4.37206	0.21353	0.27708	0.01171	0.865	yes	1871	44	1707	40	1577	59	17.7
NG043-067	87743	2	0.08245	0.00131	2.02835	0.08813	0.17843	0.00722	0.931	no	1256	31	1125	29	1058	39	17.1
NG043-063	55160	5	0.05751	0.00138	0.53669	0.02220	0.06769	0.00228	0.815	no	511	52	436	15	422	14	18.0
NG043-056	760045	3183	0.20635	0.00440	12.64723	0.55955	0.44453	0.01723	0.876	yes	2877	34	2654	41	2371	76	21.0
NG043-011	32920	20	0.07955	0.00349	1.77940	0.12464	0.16223	0.00885	0.779	no	1186	84	1038	45	969	49	19.7
NG043-085	103194	19	0.05792	0.00091	0.55045	0.02208	0.06893	0.00254	0.920	no	527	34	445	14	430	15	19.0
NG043-087	44725	30	0.08358	0.00339	1.98663	0.11303	0.17239	0.00687	0.700	no	1283	77	1111	38	1025	38	21.7
NG043-122	270256	578	0.08573	0.00369	2.08157	0.13086	0.17609	0.00807	0.729	yes	1332	81	1143	42	1046	44	23.3
NG043-027	262650	458	0.10562	0.00331	3.32514	0.19535	0.22833	0.01135	0.846	yes	1725	56	1487	45	1326	59	25.6
NG043-091	42946	44	0.08298	0.00781	1.85106	0.19435	0.16178	0.00754	0.444	no	1269	173	1064	67	967	42	25.6
NG043-006	415036	14	0.08585	0.00110	1.99794	0.11974	0.16879	0.00988	0.977	no	1335	24	1115	40	1005	54	26.6
NG043-075	2036031	16949	0.17640	0.00794	7.13775	0.59689	0.29346	0.02068	0.843	yes	2619	73	2129	72	1659	102	41.5
NG043-098	37325	17	0.06232	0.00344	0.58951	0.04143	0.06860	0.00299	0.620	no	685	114	471	26	428	18	38.8
NG043-032	132033	4228	0.12462	0.04015	3.53369	0.18714	0.07620	0.01348	0.199	yes	2023	482	1535	232	1206	72	44.2

TABLE A4

Data for NP021A Red Island Road Formation

sample name	^{206}Pb (cps)	^{204}Pb (cps)	Isotopic ratios $\frac{^{207}Pb}{^{206}Pb}$	2σ	$\frac{^{207}Pb}{^{235}U}$	2σ	$\frac{^{206}Pb}{^{238}U}$	2σ	r	Com Pb corrected	Apparent age summary age (Ma) $\frac{^{207}Pb^*}{^{206}Pb^*}$	error (Ma) 2σ	age (Ma) $\frac{^{207}Pb^*}{^{235}U}$	error (Ma) 2σ	age (Ma) $\frac{^{206}Pb^*}{^{238}U}$	error (Ma) 2σ	disc. %
Better than ± 10% discordant																	
NP021A-047	313380	137	0.07175	0.00074	1.68331	0.05792	0.17016	0.00559	0.954	no	979	21	1002	22	1013	31	-3.8
NP021A-097	55375	118	0.07297	0.00097	1.64819	0.06532	0.16382	0.00612	0.942	no	1013	27	989	25	978	34	3.7
NP021A-078	32029	275	0.07394	0.00095	1.70780	0.07371	0.16751	0.00690	0.955	no	1040	26	1011	27	998	38	4.3
NPO21A-019	78818	56	0.07428	0.00086	1.66590	0.06660	0.16265	0.00623	0.957	no	1049	23	996	25	971	34	8.0
NP021A-104	524570	165	0.07458	0.00117	1.76364	0.06468	0.17150	0.00568	0.903	no	1057	31	1032	23	1020	31	3.8
NPO21A-005	92150	63	0.07476	0.00081	1.70510	0.09539	0.16541	0.00908	0.981	no	1062	22	1010	35	987	50	7.7
NP021A-058	37586	178	0.07479	0.00093	1.82670	0.07687	0.17713	0.00712	0.955	no	1063	25	1055	27	1051	39	1.2
NP021A-060	154330	210	0.07483	0.00085	1.79607	0.06706	0.17408	0.00619	0.953	no	1064	23	1044	24	1035	34	3.0
NPO21A-012	131974	37	0.07483	0.00082	1.75717	0.06192	0.17030	0.00571	0.951	no	1064	22	1030	23	1014	31	5.1
NP021A-045	178345	150	0.07489	0.00079	1.82788	0.06150	0.17702	0.00565	0.949	no	1066	21	1056	22	1051	31	1.5
NP021A-027	55131	140	0.07492	0.00093	1.67235	0.06215	0.16189	0.00567	0.943	no	1066	25	998	23	967	31	10.0
NPO21A-061	26052	228	0.07493	0.00113	1.79382	0.07146	0.17362	0.00640	0.925	no	1067	30	1043	26	1032	35	3.5
NP021A-044	172586	164	0.07494	0.00082	1.81470	0.06191	0.17563	0.00567	0.947	no	1067	22	1051	22	1043	31	2.4
NP021A-042	34254	137	0.07501	0.00107	1.75602	0.06812	0.16979	0.00613	0.931	no	1069	28	1029	25	1011	34	5.8
NP021A-081	165844	138	0.07514	0.00087	1.82147	0.08202	0.17581	0.00765	0.967	no	1072	23	1053	29	1044	42	2.9
NP021A-098	38241	130	0.07520	0.00118	1.69924	0.06482	0.16389	0.00570	0.911	no	1074	31	1008	24	978	31	9.6
NP021A-059	33434	213	0.07525	0.00097	1.80703	0.07578	0.17416	0.00695	0.952	no	1075	26	1048	27	1035	38	4.1
NPO21A-014	53431	28	0.07527	0.00094	1.76157	0.06197	0.16974	0.00558	0.935	no	1076	25	1031	23	1011	31	6.5
NP021A-096	124920	108	0.07566	0.00098	1.88018	0.08384	0.18023	0.00769	0.957	no	1086	26	1074	29	1068	42	1.8
NP021A-006	42666	55	0.07571	0.00092	1.78000	0.09818	0.17051	0.00917	0.975	no	1087	24	1038	35	1015	50	7.2
NPO21A-064	8129	294	0.07578	0.00161	2.03148	0.09508	0.19442	0.00811	0.892	no	1089	42	1126	31	1145	44	-5.6
NP021A-100	15583	128	0.07579	0.00176	1.83496	0.07698	0.17560	0.00614	0.833	no	1089	46	1058	27	1043	34	4.6
NP021A-030	7143	164	0.07592	0.00153	1.77882	0.07968	0.16992	0.00680	0.893	no	1093	40	1038	29	1012	37	8.0
NP021A-046	429220	126	0.07593	0.00080	2.00176	0.07472	0.19120	0.00684	0.959	no	1093	21	1116	25	1128	37	-3.5
NPO21A-068	74136	307	0.07626	0.00088	1.88764	0.07315	0.17953	0.00664	0.955	no	1102	23	1077	25	1064	36	3.7
NPO21A-020	115852	101	0.07654	0.00099	1.83963	0.09107	0.17432	0.00833	0.965	no	1109	26	1060	32	1036	46	7.2
NP021A-048	34576	135	0.07656	0.00099	1.95097	0.07225	0.18483	0.00642	0.937	no	1110	26	1099	25	1093	35	1.6
NP021A-092	31343	146	0.07664	0.00103	1.98001	0.07837	0.18738	0.00698	0.941	no	1112	27	1109	26	1107	38	0.4
NP021A-101	108166	172	0.07700	0.00124	1.91439	0.07421	0.18032	0.00636	0.910	no	1121	32	1086	26	1069	35	5.1
NP021A-083	37856	117	0.07708	0.00094	1.98455	0.07794	0.18673	0.00697	0.951	no	1123	24	1110	26	1104	38	1.9
NP021A-049	628998	108	0.07709	0.00081	1.99186	0.07280	0.18740	0.00656	0.958	no	1123	21	1113	24	1107	36	1.6
NP021A-023	46075	110	0.07711	0.00096	1.81263	0.06626	0.17048	0.00586	0.941	no	1124	25	1050	24	1015	32	10.5
NP021A-102	66400	159	0.07727	0.00131	1.87167	0.07364	0.17569	0.00623	0.902	no	1128	33	1071	26	1043	34	8.1
NP021A-002	139353	89	0.07730	0.00086	1.88146	0.10446	0.17653	0.00960	0.980	no	1129	22	1075	36	1048	52	7.8
NP021A-093	338766	111	0.07731	0.00081	2.01606	0.07248	0.18913	0.00651	0.957	no	1129	21	1121	24	1117	35	1.2
NP021A-091	167442	112	0.07735	0.00085	1.98282	0.07442	0.18591	0.00667	0.956	no	1130	22	1110	25	1099	36	3.0
NP021A-111	100096	181	0.07737	0.00125	1.91218	0.06995	0.17925	0.00588	0.897	no	1131	32	1085	24	1063	32	6.5
NP021A-095	74896	112	0.07752	0.00088	1.98470	0.07217	0.18570	0.00641	0.950	no	1134	23	1110	24	1098	35	3.5
NP021A-021	81783	68	0.07759	0.00098	1.85424	0.08127	0.17332	0.00728	0.958	no	1136	25	1065	29	1030	40	10.1
NP021A-086	69583	101	0.07761	0.00090	1.99686	0.07423	0.18660	0.00659	0.950	no	1137	23	1114	25	1103	36	3.3
NP021A-090	82431	91	0.07768	0.00087	2.00609	0.07702	0.18729	0.00688	0.956	no	1139	22	1118	26	1107	37	3.1

TABLE A4
(continued)

sample name	^{206}Pb (cps)	^{204}Pb (cps)	Isotopic ratios $\frac{^{207}Pb}{^{206}Pb}$	2σ	$\frac{^{207}Pb}{^{235}U}$	2σ	$\frac{^{206}Pb}{^{238}U}$	2σ	r	Com Pb corrected	Apparent age summary age (Ma) $\frac{^{207}Pb^*}{^{206}Pb^*}$	error (Ma) 2σ	age (Ma) $\frac{^{207}Pb^*}{^{235}U}$	error (Ma) 2σ	age (Ma) $\frac{^{206}Pb^*}{^{238}U}$	error (Ma) 2σ	disc. %
Better than ± 10% discordant																	
NP021A-105	86027	161	0.07769	0.00135	1.96528	0.07859	0.18347	0.00661	0.901	no	1139	34	1104	27	1086	36	5.1
NP021A-082	89024	88	0.07773	0.00089	2.00563	0.07273	0.18713	0.00644	0.949	no	1140	23	1117	24	1106	35	3.3
NP021A-109	68345	172	0.07780	0.00131	1.94279	0.07401	0.18112	0.00619	0.897	no	1142	33	1096	25	1073	34	6.5
NP021A-026	28183	146	0.07780	0.00113	1.91963	0.07933	0.17895	0.00692	0.936	no	1142	29	1088	27	1061	38	7.6
NP021A-084	78814	113	0.07784	0.00089	2.00659	0.07363	0.18696	0.00652	0.950	no	1143	23	1118	25	1105	35	3.6
NPO21A-013	19866	54	0.07788	0.00137	2.03301	0.08015	0.18932	0.00668	0.895	no	1144	35	1127	26	1118	36	2.5
NP021A-080	262466	263	0.07790	0.00090	2.11425	0.07125	0.19685	0.00623	0.940	no	1144	23	1153	23	1158	33	-1.3
NP021A-056	336500	144	0.07792	0.00081	2.07904	0.07155	0.19352	0.00635	0.953	no	1145	21	1142	23	1140	34	0.4
NP021A-106	39086	168	0.07796	0.00136	1.98382	0.08236	0.18456	0.00695	0.907	no	1146	34	1110	28	1092	38	5.1
NPO21A-040	184871	205	0.07798	0.00083	1.99083	0.07052	0.18515	0.00625	0.953	no	1146	21	1112	24	1095	34	4.9
NP021A-107	53575	165	0.07801	0.00130	1.99811	0.07945	0.18578	0.00671	0.909	no	1147	33	1115	27	1098	36	4.6
NPO21A-038	372730	205	0.07806	0.00082	2.02108	0.07795	0.18777	0.00697	0.962	no	1149	21	1123	26	1109	38	3.7
NPO21A-063	182329	287	0.07809	0.00082	2.12231	0.07604	0.19710	0.00675	0.956	no	1149	21	1156	24	1160	36	-1.0
NPO21A-062	147856	253	0.07811	0.00084	2.05576	0.07583	0.19089	0.00674	0.957	no	1150	21	1134	25	1126	36	2.2
NP021A-103	107413	142	0.07812	0.00126	1.95010	0.07535	0.18104	0.00636	0.909	no	1150	32	1098	26	1073	35	7.3
NP021A-108	117351	144	0.07814	0.00126	1.92688	0.07750	0.17885	0.00659	0.916	no	1150	32	1090	27	1061	36	8.4
NP021A-024	158163	107	0.07817	0.00085	1.91700	0.07213	0.17787	0.00641	0.957	no	1151	21	1087	25	1055	35	9.0
NP021A-054	35091	148	0.07818	0.00099	1.98540	0.07554	0.18418	0.00661	0.943	no	1151	25	1111	25	1090	36	5.8
NP021A-074	157882	381	0.07821	0.00085	2.00967	0.08590	0.18636	0.00771	0.967	no	1152	21	1119	29	1102	42	4.8
NP021A-016	282150	61	0.07823	0.00085	2.01488	0.07851	0.18679	0.00699	0.960	no	1153	21	1121	26	1104	38	4.6
NP021A-072	20585	338	0.07826	0.00120	1.97317	0.08923	0.18285	0.00778	0.941	no	1154	30	1106	30	1083	42	6.7
NPO21A-039	105773	203	0.07833	0.00091	1.95640	0.07370	0.18115	0.00649	0.951	no	1155	23	1101	25	1073	35	7.7
NPO21A-011	78195	18	0.07834	0.00096	2.02719	0.07300	0.18768	0.00635	0.940	no	1155	24	1125	24	1109	34	4.4
NP021A-075	32840	333	0.07841	0.00104	2.05544	0.08069	0.19012	0.00702	0.941	no	1157	26	1134	26	1122	38	3.3
NP021A-099	82896	138	0.07841	0.00093	1.95970	0.07061	0.18126	0.00617	0.944	no	1157	23	1102	24	1074	34	7.8
NP021A-066	100538	294	0.07842	0.00086	2.12171	0.08531	0.19622	0.00759	0.962	no	1158	22	1156	27	1155	41	0.2
NPO21A-065	96428	268	0.07853	0.00089	2.12838	0.08000	0.19658	0.00705	0.954	no	1160	22	1158	26	1157	38	0.3
NP021A-077	146696	304	0.07857	0.00086	2.00142	0.07603	0.18474	0.00672	0.957	no	1161	22	1116	25	1093	36	6.4
NPO21A-034	46967	238	0.07861	0.00104	1.92202	0.07264	0.17733	0.00628	0.937	no	1162	26	1089	25	1052	34	10.2
NPO21A-069	25760	290	0.07867	0.00105	2.01453	0.07903	0.18572	0.00686	0.941	no	1164	26	1120	26	1098	37	6.1
NPO21A-017	121168	46	0.07869	0.00090	2.02632	0.07954	0.18677	0.00701	0.956	no	1164	23	1124	26	1104	38	5.6
NP021A-029	44172	176	0.07870	0.00102	1.95133	0.07828	0.17982	0.00683	0.946	no	1165	25	1099	27	1066	37	9.2
NPO21A-004	68082	60	0.07871	0.00090	2.00196	0.11382	0.18447	0.01027	0.980	no	1165	23	1116	38	1091	56	6.9
NP021A-043	52489	161	0.07876	0.00089	2.04692	0.07918	0.18849	0.00697	0.956	no	1166	22	1131	26	1113	38	4.9
NPO21A-018	76047	68	0.07881	0.00090	1.96104	0.07451	0.18048	0.00654	0.953	no	1167	23	1102	25	1070	36	9.1
NP021A-022	206661	101	0.07883	0.00087	1.94186	0.07148	0.17867	0.00628	0.954	no	1168	22	1096	24	1060	34	10.0
NP021A-055	63160	164	0.07884	0.00094	2.01997	0.07109	0.18582	0.00615	0.941	no	1168	23	1122	24	1099	33	6.5
NPO21A-007	82459	64	0.07910	0.00089	1.99835	0.11333	0.18323	0.01018	0.980	no	1175	22	1115	38	1085	55	8.3
NPO21A-015	39544	21	0.07916	0.00110	1.96788	0.07823	0.18030	0.00672	0.937	no	1176	27	1105	26	1069	37	9.9
NP021A-110	24874	179	0.07917	0.00151	1.97288	0.08390	0.18073	0.00686	0.893	no	1176	37	1106	28	1071	37	9.7
NP021A-053	55210	135	0.07934	0.00101	2.09233	0.08632	0.19127	0.00751	0.951	no	1181	25	1146	28	1128	40	4.8

TABLE A4
(continued)

sample name	^{206}Pb (cps)	^{204}Pb (cps)	Isotopic ratios $\frac{^{207}Pb}{^{206}Pb}$	2σ	$\frac{^{207}Pb}{^{235}U}$	2σ	$\frac{^{206}Pb}{^{238}U}$	2σ	r	Com Pb corrected	Apparent age summary age (Ma) $\frac{^{207}Pb^*}{^{206}Pb^*}$	error (Ma) 2σ	age (Ma) $\frac{^{207}Pb^*}{^{235}U}$	error (Ma) 2σ	age (Ma) $\frac{^{206}Pb^*}{^{238}U}$	error (Ma) 2σ	disc. %
Better than ± 10% discordant																	
NP021A-052	14021	122	0.07973	0.00151	2.14244	0.09286	0.19489	0.00760	0.900	no	1190	37	1163	30	1148	41	3.9
NP021A-076	28024	308	0.08012	0.00121	2.06481	0.08227	0.18690	0.00689	0.926	no	1200	29	1137	27	1105	37	8.7
NPO21A-003	30747	60	0.08020	0.00145	2.04537	0.11660	0.18497	0.01000	0.949	no	1202	35	1131	38	1094	54	9.7
NP021A-051	64374	114	0.08030	0.00121	2.05845	0.07482	0.18592	0.00615	0.910	no	1204	29	1135	25	1099	33	9.5
NPO21A-067	17771	275	0.08051	0.00185	2.19469	0.09346	0.19771	0.00708	0.841	no	1209	45	1179	29	1163	38	4.2
NP021A-071	48475	315	0.08067	0.00099	2.08619	0.08355	0.18756	0.00715	0.952	no	1213	24	1144	27	1108	39	9.4
NP021A-050	277097	134	0.08174	0.00097	2.16609	0.07902	0.19219	0.00663	0.946	no	1239	23	1170	25	1133	36	9.3
NP021A-057	528704	186	0.08193	0.00085	2.46447	0.08753	0.21816	0.00741	0.957	no	1244	20	1262	25	1272	39	-2.5
NP021A-079	415392	286	0.08218	0.00086	2.48970	0.09584	0.21972	0.00814	0.962	no	1250	20	1269	28	1280	43	-2.7
NP021A-025	231552	149	0.09229	0.00103	3.04875	0.11556	0.23959	0.00868	0.956	no	1473	21	1420	29	1385	45	6.7
NPO21A-009	369707	40	0.09761	0.00103	3.47481	0.19100	0.25818	0.01393	0.981	no	1579	20	1522	42	1481	71	7.0
NP021A-089	273009	86	0.10053	0.00107	3.84455	0.13474	0.27737	0.00926	0.953	no	1634	20	1602	28	1578	47	3.8
NP021A-088	59006	119	0.10358	0.00136	4.26713	0.17869	0.29878	0.01188	0.950	no	1689	24	1687	34	1685	59	0.3
NP021A-094	119456	100	0.11219	0.00121	4.94015	0.18422	0.31937	0.01140	0.958	no	1835	19	1809	31	1787	55	3.0
NP021A-041	205737	144	0.11294	0.00117	5.16602	0.19209	0.33175	0.01185	0.960	no	1847	19	1847	31	1847	57	0.0
NPO21A-008	153471	46	0.11406	0.00122	4.91643	0.27977	0.31262	0.01747	0.982	no	1865	19	1805	47	1754	85	6.8
Discordance >10% or <-10%																	
NP021A-087	5758	92	0.07078	0.00215	1.73483	0.09557	0.17776	0.00817	0.834	no	951	61	1022	35	1055	45	-11.8
NPO21A-032	68494	228	0.07930	0.00090	1.94509	0.06766	0.17789	0.00585	0.945	no	1180	22	1097	23	1055	32	11.4
NPO21A-035	35104	225	0.07933	0.00108	1.93766	0.07469	0.17715	0.00639	0.935	no	1180	27	1094	25	1051	35	11.8
NPO21A-037	32106	239	0.07958	0.00104	1.95425	0.07758	0.17810	0.00668	0.945	no	1187	25	1100	26	1057	36	11.9
NP021A-085	24244	120	0.08379	0.00264	2.24053	0.11355	0.19393	0.00770	0.783	no	1288	60	1194	35	1143	41	12.3
NPO21A-001	92185	68	0.07931	0.00088	1.92699	0.10976	0.17622	0.00984	0.981	no	1180	22	1090	37	1046	54	12.3
NPO21A-036	98830	263	0.07884	0.00106	1.89485	0.06754	0.17432	0.00576	0.926	no	1168	26	1079	23	1036	32	12.2
NP021A-028	23015	149	0.07991	0.00125	1.95564	0.06958	0.17750	0.00567	0.898	no	1195	31	1100	24	1053	31	12.8
NPO21A-033	220136	212	0.07777	0.00087	1.80885	0.07097	0.16870	0.00634	0.958	no	1141	22	1049	25	1005	35	12.9
NPO21A-010	156764	56	0.07641	0.00127	1.70826	0.10644	0.16215	0.00974	0.964	no	1106	33	1012	39	969	54	13.3
NP021A-073	60824	376	0.08191	0.00118	2.06629	0.07873	0.18295	0.00645	0.925	no	1243	28	1138	26	1083	35	14.0
NPO21A-031	28174	197	0.08167	0.00226	1.98462	0.08912	0.17625	0.00623	0.787	no	1238	53	1110	30	1046	34	16.7

TABLE A5

U-Pb Zircon Data for Rhyolite Cobble from Red Island, Newfoundland

Fraction				Weight	Concentration U	Concentration Pb_{rad}	Measured Total Common Pb $\frac{^{206}Pb}{^{204}Pb}$	Corrected Atomic Ratios * $\frac{^{208}Pb}{^{206}Pb}$	$\frac{^{206}Pb}{^{208}U}$	+/-	$\frac{^{207}Pb}{^{205}U}$	+/-	$\frac{^{207}Pb}{^{206}Pb}$	+/-	Age [Ma] $\frac{^{206}Pb}{^{238}U}$	$\frac{^{207}Pb}{^{235}U}$	$\frac{^{207}Pb}{^{206}Pb}$
				mg	ppm		pg										
Z1	4	euh	prm	0.006	888	68.8	1422	0.1126	0.07690	56	0.6340	44	0.05980	32	478	499	596
Z2	3	euh	prm	0.004	794	54.5	222	0.1255	0.06756	30	0.5210	76	0.05593	74	421	426	450
Z3	2	euh	prm	0.003	1150	82.0	857	0.1240	0.06993	38	0.5906	52	0.06125	44	436	471	648
Z4	3	euh	prm	0.004	1291	88.4	1965	0.1263	0.06741	34	0.5135	26	0.05525	14	421	421	423

Notes: Z=zircon, 2,3,4=number of grains, euh=euhedral, prm=prism.

All zircon was chemically abraded (Mattinson, 2005). Weights were estimated so U and Pb concentrations are approximate.

* Atomic ratios corrected for fractionation, spike, laboratory blank of 1-2 picograms of common lead, and initial common lead at the age of the sample calculated from the model of Stacey and Kramers (1975), and 0.3 picogram U blank. Two sigma uncertainties are reported after the ratios and refer to the final digits.

REFERENCES

Allen, J. S., ms, 2009, Paleogeographic Reconstruction of the St. Lawrence Promontory, Western Newfoundland: Lexington, Kentucky, University of Kentucky, Ph. D. thesis, 288 p.

Allen, J. S., Thomas, W. A., and Lavoie, D., 2010, The Laurentian margin of northeastern North America, *in* Tollo, R. P., Bartholomew, M. J., Hibbard, J. P., and Karabinos, P. M., editors, From Rodinia to Pangea: The Lithotectonic Record of the Appalachian Region: Geological Society of America Memoir 206, p. 71–90, https://doi.org/10.1130/2010.1206(04)

Ashton, K. E., Heaman, L. M., Lewry, J. F., Hartlaub, R. P., and Shi, R., 1999, Age and origin of the Jan Lake Complex: A glimpse at the buried Archean craton of the Trans-Hudson Orogen: Canadian Journal of Earth Sciences, v. 36, n. 2, p. 185–208, https://doi.org/10.1139/cjes-36-2-185

Bashforth, A. R., ms, 1995, Provenance of the Red Island Road Formation, western Newfoundland: Brandon, Manitoba, Canada, Brandon University, B. Sc. thesis.

Batten Hender, K. L., and Dix, G. R., 2008, Facies development of a Late Ordovician mixed carbonate-siliciclastic ramp proximal to the developing Taconic orogen: Lourdes Formation, Newfoundland, Canada: Facies, v. 54, n. 1, p. 121–149, https://doi.org/10.1007/s10347-007-0126-0

Bergström, S. M., Riva, J., and Kay, M., 1974, Significance of conodonts, graptolites, and shelly faunas from the Ordovician of western and north-central Newfoundland: Canadian Journal of Earth Sciences, v. 11, n. 12, p. 1625–1660, https://doi.org/10.1139/e74-163

Bird, J. M., and Dewey, J. F., 1970, Lithosphere plate-continental margin tectonics and the evolution of the Appalachian orogen: GSA Bulletin, v. 81, n. 4, p. 1031–1060, https://doi.org/10.1130/0016-7606(1970)81[1031:LPMTAT]2.0.CO;2

Bradley, D. C., 1983, Tectonics of the Acadian orogeny in New England and adjacent Canada: The Journal of Geology, v. 91, n. 4, p. 381–400, https://doi.org/10.1086/628785

Bradley, D. C., and Kidd, W. S. F., 1991, Flexural extension of the upper continental crust in collisional foredeeps: GSA Bulletin, v. 103, n. 1, p. 1416–1438, https://doi.org/10.1130/0016-7606(1991)103<1416:FEOTUC>2.3.CO;2

Burden, E. T., Quinn, L., Nowlan, G. S., and Bailey-Nill, L. A., 2002, Palynology and micropaleontology of the Clam Bank Formation (Lower Devonian) of western Newfoundland, Canada: Palynology, v. 26, n. 1, p. 185–215, https://doi.org/10.1080/01916122.2002.9989572

Calvert, A. J., and Ludden, J. N., 1999, Archean continental assemby in the southeastern Superior Province of Canada: Tectonics, v. 18, n. 3, p. 412–429, https://doi.org/10.1029/1999TC900006

Cawood, P. A., and Nemchin, A. A., 2001, Paleogeographic development of the east Laurentian margin: Constraints from U-Pb dating of detrital zircons in the Newfoundland Appalachians: GSA Bulletin, v. 113, n. 9, p. 1234–1246, https://doi.org/10.1130/0016-7606(2001)113<1234:PDOTEL>2.0.CO;2

Cawood, P. A., and Williams, H., 1988, Acadian basement thrusting, crustal delamination, and structural styles in and around the Humber Arm allochthon, western Newfoundland: Geology, v. 16, n. 4, p. 370, https://doi.org/10.1130/0091-7613(1988)016<0370:ABTCDA>2.3.CO;2

Cawood, P. A., Dunning, G. R., Lux, D., and van Gool, J. A. M., 1994, Timing of peak metamorphism and deformation along the Appalachian margin of Laurentia in Newfoundland: Silurian, not Ordovician: Geology, v. 22, n. 5, p. 399–402, https://doi.org/10.1130/0091-7613(1994)022<0399:TOPMAD>2.3.CO;2

Cawood, P. A., McCausland, P. J., and Dunning, G. R., 2001, Opening Iapetus: Constraints from the Laurentian margin in Newfoundland: GSA Bulletin, v. 113, n. 4, p. 443–453, https://doi.org/10.1130/0016-7606(2001)113<0443:OICFTL>2.0.CO;2

Cawood, P. A., Nemchin, A. A., and Stachan, R., 2007a, Provenance record of Laurentian passive-margin strata in the northern Caledonides: Implications for paleodrainage and paleogeography: GSA Bulletin, v. 119, n. 7–8, p. 993–1003, https://doi.org/10.1130/B26152.1

Cawood, P. A., Nemchin, A. A., Strachan, R., Prave, T., and Krabbendam, M., 2007b, Sedimentary basin and detrital zircon record along East Laurentia and Baltica during assembly and breakup of Rodinia: Journal of the Geological Society, v. 164, n. 2, p. 257–275 https://doi.org/10.1144/0016-76492006-115

Chow, N., and James, N. P., 1987, Cambrian Grand Cycles: A northern Appalachian perspective: GSA Bulletin, v. 98, n. 4, p. 418, https://doi.org/10.1130/0016-7606(1987)98<418:CGCANA>2.0.CO;2

Corfu, F., and Lin, S., 2000, Geology and U-Pb geochronology of the Island Lake greenstone belt, northwestern Superior Province, Manitoba: Canadian Journal of Earth Sciences, v. 37, n. 9, p. 1275–1286, https://doi.org/10.1139/e00-043

Dewey, J. F., and Bird, J. M., 1971, Origin and Emplacement of the Ophiolite Suite: Appalachian Ophiolites in Newfoundland: Journal of Geophysical Research, v. 76, n. 14, p. 3179–3206, https://doi.org/10.1029/JB076i014p03179

Dewery, J. F., and Casey, J. F., 2013, The sole of an ophiolite: The Ordovician Bay of Islands Complex, Newfoundland: Journal of the Geological Society, v. 170, n. 5, p. 715–722, https://doi.org/10.1144/jgs2013-017

Downey, M. W., Lin, S., Böhm, C. O., and Rayner, N. M., 2009, Timing and kinematics of crustal movement in the Northern Superior superterrane: Insights from the Gull Rapids area of the Split Lake Block, Manitoba: Precambrian Research, v. 168, n. 1–2, p. 134–148, https://doi.org/10.1016/j.precamres.2008.04.009

Dunning, G. R., and Krogh, T. E., 1985, Geochronology of ophiolites of the Newfoundland Appalachians: Canadian Journal of Earth Sciences, v. 22, n. 11. p. 1659–1670. https://doi.org/10.1139/e85-174

Dunning, G. R., O'Brien, S. J., Colman-Sadd, S. P., Blackwood, R. F., Dickson, W. L., O'Neill, P. P. O., and Krogh, T. E., 1990, Silurian orogeny in the Newfoundland Appalachians: The Journal of Geology, v. 98, n. 6, . 895–913, https://doi.org/10.1086/629460

Elhlou, S., Belousova, E., Griffin, W. L., Pearson, N. J., and O'Reilly, S. Y., 2006, Trace element and isotopic

composition of GJ-red zircon standard by laser ablation: Geochimica et Cosmochimica Acta, v. 70, n. 18, p. A158, https://doi.org/10.1016/j.gca.2006.06.1383
Fåhraeus, L. E., 1966, Lower Viruan (Middle Ordovician) conodonts from the Gullhogen quarry, southern central Sweden: Sveriges Geologiska Undersokning Series C, v. 610, p. 1–40.
Gaudette, H. E., Vitrac-Michard, A., and Allègre, C. J., 1981, North American Precambrian history recorded in a single sample: High-resolution U-Pb systematics of the Potsdam sandstone detrital zircons, New York State: Earth and Planetary Science Letters, v. 54, n. 2, p. 248–260, https://doi.org/10.1016/0012-821X(81)90008-X
Gehrels, G., Valencia, V., and Pullen, A., 2006, Detrital zircon geochronology by laser ablation multicollector ICPMS at the Arizona Laserchron Center, *in* Olszewski, T. D., editor, Geochronology: Emerging opportunities: The Paleontological Society Papers, v. 12, p. 67–76, https://doi.org/10.1017/S1089332600001352
Heamn, L. M., Erdmer, P., and Owen, J. V., 2002, U–Pb geochronologic constraints on the crustal evolution of the Long Range Inlier, Newfoundland: Canadian Journal of Earth Sciences, v. 39, n. 5, p. 845–865, https://doi.org/10.1139/e02-015
Hiscott, R. N., 1978, Provenance of Ordovician deep-water sandstones, Tourelle Formation, Quebec, and implications for initiation of the Taconic orogeny: Canadian Journal of Earth Sciences, v. 15, n. 10, p. 1579–1597, https://doi.org/10.1139/e78-163
——— 1984, Ophiolitic source rocks for Taconic-age flysch: Trace-element evidence: GSA Bulletin, v. 95, n. 11, p. 1261–1267, https://doi.org/10.1130/0016-7606(1984)95<1261:OSRFTF>2.0.CO;2
Hoffman, P. F., 1988, United Plates of America, The Birth of a Craton: Early Proterozoic Assembly and Growth of Laurentia: Annual Review of Earth and Planetary Sciences, v. 16, p. 543–603, https://doi.org/10.1146/annurev.earth.16.1.543
Ibañez-Mejia, M., Pullen, A., Pepper, M., Urbani, F., Ghoshal, G., and Ibañez-Meijia, J. C., 2018, Use and abuse of detrital zircon U-Pb geochronology—A case from the Río Orinoco delta, eastern Venezuela: Geology, v. 46, n. 11, p. 1019–1022, https://doi.org/10.1130/G45596.1
Jackson, S. E., Pearson, N. J., Griffin, W. L., and Belousova, E. A., 2004, The application of laser ablation-inductively coupled plasma-mass spectrometry to *in situ* U–Pb zircon geochronology: Chemical Geology, v. 211, n. 1–2, p. 47–69, https://doi.org/10.1016/j.chemgeo.2004.06.017
Jenner, G. A., Dunning, G. R., Malpas, J., Brown, M., and Brace, T., 1991, Bay of Islands and Little Port complexes, revisited: Age, geochemical and isotopic evidence confirm suprasubduction-zone origin: Canadian Journal of Earth Sciences, v. 28, n. 10, p. 1635–1652, https://doi.org/10.1139/e91-146
Karabinos, P., Aleinikoff, J. N., and Fanning, C. M., 1999, Distinguishing Grenvillian basement from pre-Taconian cover rocks in the northern Appalachians: American Journal of Science, v. 299, n. 6, p. 502–515, https://doi.org/10.2475/ajs.299.6.502
Karabinos, P., Macdonald, F. A., and Crowley, J. L., 2017, Bridging the gap between the foreland and hinterland I: Geochronology and plate tectonic geometry of Ordovician magmatism and terrane accretion on the Laurentian margin of New England: American Journal of Science, v. 317, n. 5, p. 515–554, https://doi.org/10.2475/05.2017.01
Knight, I., and James, N. P., 1987, The stratigraphy of the Lower Ordovician St. George Group, western Newfoundland: The interaction between eustasy and tectonics: Canadian Journal of Earth Sciences, v. 24, n. 10, p. 1927–1951, https://doi.org/10.1139/e87-185
Knight, I., James, N. P., and Lane, T. E., 1991, The Ordovician St. George Unconformity, northern Appalchians: The relationship of plate convergence at the St. Lawrence Promontory to the Sauk/Tippecanoe sequence boundary: GSA Bulletin, v. 103, n. 9, p. 1200–1225, https://doi.org/10.1130/0016-7606(1991)103<1200:TOSGUN>2.3.CO;2
Lin, S., Davis, D. W., Barr, S. M., van Staal, C. R., Chen, Y., and Constantin, M., 2007, U-Pb geochronological constraints on the evolution of the Aspy terrane, Cape Breton Island: Implications for relationships between ASPY and BRAS D'OR terranes and Ganderia in the Canadian Appalachians: American Journal of Science, v. 307, n. 2, p. 371–398, https://doi.org/10.2475/02.2007.03
Ludwig, K. R., 2012, User's manual for Isoplot 3.75: Berkeley Ceochronology Center Special Publication, v. 5, p. 75.
Macdonald, F. A., Ryan-Davis, J., Coish, R. A., Crowley, J. L., and Karabinos, P., 2014, A newly identified Gondwanan terrane in the northern Appalachian Mountains: Implications for the Taconic orogeny and closure of the Iapetus Ocean: Geology, v. 42, n. 6, p. 539–542, https://doi.org/10.1130/G35659.1
Macdonald, F. A., Karabinos, P. M., Crowley, J. L., Hodgin, E. B., Crockford, P. W., and Delano, J. W., 2017, Bridging the gap between the foreland and hinterland II: Geochronology and tectonic setting of Ordovician magmatism and basin formation on the Laurentian margin from New England to Newfoundland: American Journal of Science, v. 317, n. 5, p. 555–596, https://doi.org/10.2475/05.2017.02
Mattinson, J. M., 2005, Zircon U–Pb chemical abrasion ("CA-TIMS") method: Combined annealing and multi-step partial dissolution analysis for improved precision and accuracy of zircon ages: Chemical Geology, v. 220, n. 1–2, p. 47–66, https://doi.org/10.1016/j.chemgeo.2005.03.011
McDaniel, D. K., Hanson, G. N., McLennan, S. M., and Sevigny, J. H., 1997, Grenvillian provenance for the amphibolite-grade Trap Falls Formation: Implications for early Paleozoic tectonic history of New England: Canadian Journal of Earth Sciences, v. 34, n. 9, p. 1286–1294, https://doi.org/10.1139/e17-102
McLennan, S. M., Bock, B., Compston, W., Hemming, S. R., and McDaniel, D. K., 2001, Detrital zircon geochronology of Taconian and Acadian foreland sedimentary rocks in New England: Journal of Sedimentary Research, v. 71, n. 2, p. 305–317, https://doi.org/10.1306/072600710305
Melchin, M. J., Sadler, P. M., Cramer, B. D., Cooper, R. A., Gradstein, F. M., and Hammer, O., 2012, The Silurian Period, *in* Gradstein, F. M., Ogg, J. G., Schmidtz, M., and Ogg, G. editors, The Geologic Time Scale 2012: Amsterdam, Elsevier, p. 525–558, https://doi.org/10.1016/B978-0-444-59425-9.00021-4

Miller, B. V., ms, 1997, Geology, geochronology, and tectonic significance of the Blair River Inlier, northern Cape Breton Island, Nova Scotia: Halifax, Nova Scotia, Dalhousie University, Ph. D. thesis, 440 p., http://hdl.handle.net/10222/55493

Miller, B. V., and Barr, S. M., 2000, Petrology and Isotopic Composition of the Grenvillian Basement Fragment in the Northern Appalachian Orogen: Blair River Inlier, Nova Scotia, Canada: Journal of Petrology, v. 41, n. 12, p. 1777–1804, https://doi.org/10.1093/petrology/41.12.1777

Miller, B. V., Dunning, G. R., Barr, S. M., Raeside, R. P., Jamieson, R. A., and Reynolds, P. H., 1996, Magmatism and metamorphism in a Grenvillian fragment: U-Pb and $^{40}Ar/^{39}Ar$ ages from the Blair River Complex, northern Cape Breton Island, Nova Scotia, Canada: GSA Bulletin, v. 108, n. 2, p. 127–140, https://doi.org/10.1130/0016-7606(1996)108<0127:MAMIAG>2.3.CO;2

Murphy, J. B., van Staal, C. R., and Keppie, J. D., 1999, Middle to late Paleozoic Acadian orogeny in the northern Appalachians: A Laramide-style plume-modified orogeny?: Geology, v. 27, n. 7, p. 653–656, https://doi.org/10.1130/0091-7613(1999)027<0653:MTLPAO>2.3.CO;2

Naylor, M., and Sinclair, H. D., 2008, Pro- vs. retro-foreland basins: Basin Research, v. 20, n. 3, p. 285–303, https://doi.org/10.1111/j.1365-2117.2008.00366.x

Nutman, A. P., Kalsbeek, F., and Friend, C. R. L., 2008, The Nagssugtoqidian orogen in South-East Greenland: Evidence for Paleoproterozoic collision and plate assembly: American Journal of Science, v. 308, n. 4, p. 529–572, https://doi.org/10.2475/04.2008.06

O'Brien, B., and O'Brien, S., 1989, Geology of the Western Hermitage Flexure: Bay D'est fault and south (Parts of 11 O/9, 11 O/16, 11 P/12 and 11 P/13), southwest Newfoundland: Map 89-133, Scale:1:100 000.

Palmer, S. E., Burden, E., and Waldron, J. W. F., 2001, Stratigraphy of the Curling Group (Cambrian), Humber Arm Allochthon, Bay of Islands: Current Research Newfoundland Department of Mines and Energy Geological Survey, Report 2001–1, p. 105–112.

Pothier, H. D., Waldron, J. W. F., Schofield, D. I., and DuFrance, S. A., 2015, Peri-Gondwanan terrane interactions recorded in the Cambrian-Ordovician detrital zircon geochronology of North Wales: Gondwana Research, v. 28, n. 3, p. 987–1001, https://doi.org/10.1016/j.gr.2014.08.009

Quinn, L. A., ms, 1992, Foreland and trench slope basin sandstones of the Goose Tickle group and Lower Head Formation, western Newfoundland: St. John's, Newfoundland, Canada, Memorial University of Newfoundland, St. John's Newfoundland, Ph. D. Thesis, 591 p.

Quinn, L., Williams, S. H., Harper, D. A. T., and Clarkson, E. N. K., 1999, Late Ordovician foreland basin fill: Long Point Group of onshore western Newfoundland: Bulletin of Canadian Petroleum Geology, v. 47, n. 1, p. 63–80.

Quinn, L., Bashforth, A. R., Burden, E. T., Gillespie, H., Springer, R. K., and Williams, S. H., 2004, The Red Island Road Formation: Early Devonian terrestrial fill in the Anticosti Foreland Basin, western Newfoundland: Canadian Journal of Earth Sciences, v. 41, n. 5, p. 587–602, https://doi.org/10.1139/e04-021

Rivers, T., 1997, Lithotectonic elements of the Grenville Province: Review and tectonic implications: Precambrian Research, v. 86, n. 3–4, p. 117–154, https://doi.org/10.1016/S0301-9268(97)00038-7

——— 2009, The Grenville Province as a large hot long-duration collisional orogen – insights from the spatial and thermal evolution of its orogenic fronts, *in* Murphy, J. B., Keppie, J. D., and Hynes, A. J. editors, Ancient Orogens and Modern Analogues: Geological Society, London, Special Publications, v. 327, p. 405–444, https://doi.org/10.1144/SP327.17

——— 2015, Tectonic Setting and Evolution of the Grenville Orogen: An Assessment of Progress Over the Last 40 Years: Geoscience Canada, v. 42, n. 1,p. 77–124, https://doi.org/10.12789/geocanj.2014.41.057

Simonetti, A., Heaman, L. M., Hartlaub, R. P., Creaser, R. A., MacHattie, T. G., and Böhm, C., 2005, U–Pb zircon dating by laser ablation-MC-ICP-MS using a new multiple ion counting Faraday collector array: Journal of Analytical Atomic Spectrometry, v. 20, n. 8, p. 677, https://doi.org/10.1039/b504465k

Sparkes, G. W., and Dunning, G. R., 2014, Late Neoproterozoic epithermal alteration and mineralization in the western Avalon Zone: A summary of mineralogical investigations and new U/Pb geochronological results: Current Research, Newfoundland and Labrador Department of Natural Resources Geological Survey, Report 14–1, p. 99–128.

Stacey, J. S., and Kramers, J. D., 1975, Approximation of terrestrial lead isotope evolution by a two-stage model: Earth and Planetary Science Letters, v. 26, n. 2, p. 207–221, https://doi.org/10.1016/0012-821X(75)90088-6

St. Julien, P., and Hubert, C., 1975, Evolution of the Taconian orogen in the Quebec Appalachians: American Journal of Science, v. 275- A, p. 337–362.

Stenzel, S. R., Knight, I., and James, N. P., 1990, Carbonate platform to foreland basin: Revised stratigraphy of the Table Head Group (Middle Ordovician), western Newfoundland: Canadian Journal of Earth Sciences, v. 27, n. 1, p. 14–26, https://doi.org/10.1139/e90-002

Stevens, R. K., 1970, Cambro-Ordovician flysch sedimentation and tectonics in West Newfoundland and their possible bearing on a Proto-Atlantic Ocean, *in* Lajoie, J., editor, Flysch sedimentology in North America: Geological Association of Canada Special Paper 7, p. 165–177.

St-Onge, M. R., Van Gool, J. A. M., Garde, A. A., and Scott, D. J., 2009, Correlation of Archaean and Palaeoproterozoic units between northeastern Canada and western Greenland: Constraining the pre-collisional upper plate accretionary history of the Trans-Hudson orogen: Geological Society, London, Special Publications, v. 318, p. 193–235, https://doi.org/10.1144/SP318.7

Thomas, W. A., and Becker, T. P., 2007, Crustal recycling in the Appalachian foreland, *in* Hatcher Jr., R. D., Carlson, M. P., McBride, J. H., and Martinez Catalan, J. R., editors, 4-D Framework of Continental Crust: Geological Society of America Memoirs, v. 200, p. 33–40, https://doi.org/10.1130/2007.1200(03)

van Staal, C. R., Dewey, J. F., MacNiocaill, C., and McKerrow, W. S., 1998, The Cambrian-Silurian tectonic evolution of the northern Appalachians and British Caledonides: History of a complex, west and

southwest Pacific-type segment of Iapetus, *in* Blundell, D. J., and Scott, A. C., editors, Lyell: the Past is the Key to the Present: Geological Society, London, Special Publications, v. 143, p. 199–242, https://doi.org/10.1144/GSL.SP.1998.143.01.17

van Staal, C. R., Whalen, J. B., McNicoll, V. J., Pehrsson, S., Lissenberg, C. J., Zagorevski, A., van Breemen, O., and Jenner, G. A., 2007, The Notre Dame arc and the Taconic orogeny in Newfoundland, *in* Hatcher, R. D., Carlson, M. P., McBride, J. H., and Martinez Catalan, J. R., editors, 4-D Framework of Continental Crust: Geological Society of America Memoir 200, p. 511–552, https://doi.org/10.1130/2007.1200(26)

van Staal, C. R., Whalen, J. B., Valverde-Vaquero, P., Zagorevski, A., and Rogers, N., 2009, Pre-Carboniferous, episodic accretion-related, orogenesis along the Laurentian margin of the northern Appalachians, *in* Murphy, J. B., Keppie, J. D., and Hynes, A. J., editors, Ancient Orogens and Modern Analogues: Geological Society, London, Special Publications, v. 327, p. 271–316, https://doi.org/10.1144/SP327.13

van Staal, C. R., Chew, D. M., Zagorevski, A., McNicoll, V., Hibbard, J., Skulski, T., Castonguay, S., Escayola, M. P., and Sylvester, P. J., 2013, Evidence of Late Ediacaran Hyperextension of the Laurentian Iapetan Margin in the Birchy Complex, Baie Verte Peninsula, Northwest Newfoundland: Implications for the Opening of Iapetus, Formation of Peri-Laurentian Microcontinents and Taconic – Grampian Orogenesis: Geoscience Canada, v. 40, n. 2, p. 94, https://doi.org/10.12789/geocanj.2013.40.006

van Staal, C. R., Zagorevski, A., McNicoll, V. J., and Rogers, N., 2014, Time-Transgressive Salinic and Acadian Orogenesis, Magmatism and Old Red Sandstone Sedimentation in Newfoundland: Geoscience Canada, v. 41, n. 2, p. 138, https://doi.org/10.12789/geocanj.2014.41.031

Vermeesch, P., 2018, Dissimilarity measures in detrital geochronology: Earth-Science Reviews, v. 178, p. 310–321, https://doi.org/10.1016/j.earscirev.2017.11.027

Waldron, J. W. F., and van Staal, C. R., 2001, Taconian orogeny and the accretion of the Dashwoods block: A peri-Laurentian microcontinent in the Iapetus Ocean: Geology, v. 29, n. 9, p. 811–814, https://doi.org/10.1130/0091-7613(2001)029<0811:TOATAO>2.0.CO;2

Waldron, J. W. F., Murphy, J. B., Melchin, M. J., and Davis, G., 1996, Silurian tectonics of western Avalonia: Strain-corrected subsidence history of the Arisaig Group, Nova Scotia: The Journal of Geology, v. 104, n. 6, p. 677–694, https://doi.org/10.1086/629862

Waldron, J. W. F., Henry, A. D., Bradley, J. C., and Palmer, S. E., 2003, Development of a folded thrust stack: Humber Arm Allochthon, Bay of Islands, Newfoundland Appalachians: Canadian Journal of Earth Sciences, v. 40, n. 2, p. 237–253, https://doi.org/10.1139/e02-042

Waldron, J. W. F., Floyd, J. D., Simonetti, A., and Heaman, L. M., 2008, Ancient Laurentian detrital zircon in the closing Iapetus Ocean, Southern Uplands terrane, Scotland: Geology, v. 36, n. 7, p. 527–530, https://doi.org/10.1130/G24763A.1

Waldron, J. W. F., McNicoll, V. J., and van Staal, C. R., 2012, Laurentia-derived detritus in the Badger Group of central Newfoundland: Deposition during closing of the Iapetus Ocean: Canadian Journal of Earth Sciences, v. 49, n. 1, p. 207–221, https://doi.org/10.1139/e11-030

Waldron, J. W. F., Schofield, D. I., DuFrane, S. A., Floyd, J. D., Crowley, Q. G., Simonetti, A., Dokken, R. J., and Pothier, H. D., 2014, Ganderia-Laurentia collision in the Caledonides of Great Britain and Ireland: Journal of the Geological Society, v. 171, p. 555–569, https://doi.org/10.1144/jgs2013-131

Waldron, J. W. F., Barr, S. M., Park, A. F., White, C. E., and Hibbard, J. P., 2015, Late Paleozoic strike-slip faults in Maritime Canada and their role in the reconfiguration of the northern Appalachian orogen: Tectonics, v. 34, n. 8, p. 1661–1684, https://doi.org/10.1002/2015TC003882

Waldron, J. W. F., Schofield, D. I., and Murphy, J. B., 2019, Diachronous Paleozoic accretion of peri-Gondwanan terranes at the Laurentian margin, *in* Wilson, R. W., Houseman, G. A., McCaffrey, K. J. W., Doré, A. G., and Buiter, S. J. H., editors, Fifty Years of the Wilson Cycle Concept in Plate Tectonics: Geological Society, London, Special Publications, v. 470, https://doi.org/10.1144/SP470.11

Whalen, J. B., Jenner, G. A., Longstaffe, F. J., Gariepy, C., and Fryer, B. J., 1997, Implications of granitoid geochemical and isotopic (Nd, O, Pb) data from the Cambrian-Ordovician Notre Dame Arc for the evolution of the Central Mobile belt, Newfoundland Appalachians, *in* Sinha, A. K., Whalen, J. B., and Hogan, J. P. editors, The Nature of Magmatism in the Appalachian Orogen: Geological Society of America Memoir 191, p. 367–395, https://doi.org/10.1130/0-8137-1191-6.367

White, S. E., ms, 2017, Evolution of the western Newfoundland Appalachian orogen and its foreland basin: Edmonton, Alberta, Canada, University of Alberta, Ph. D. Thesis, 229 p.

White, S. E., and Waldron, J. W. F., 2019, Inversion of Taconian Extensional Structures During Acadian Orogenesis in Western Newfoundland, *in* Wilson, R. W., Houseman, G. A., McCaffrey, K. J. W., Doré, A. G., and Buiter, S. J. H., editors, Tectonic evolution: 50 years of the Wilson Cycle concept: Geological Society, London, Special Publication, v. 470, https://doi.org/10.1144/SP470.17

White, S. E., Waldron, J. W. F., and Harris, N. B., 2019, Anticosti Foreland Basin Offshore of Western Newfoundland: Concealed Record of Northern Appalachian Orogen Development: Basin Research, https://doi.org/10.1111/bre.12364

Whitmeyer, S. J., and Karlstrom, K. E., 2007, Tectonic model for the Proterozoic growth of North America: Geosphere, v. 3, n. 4, p. 220–259, https://doi.org/10.1130/GES00055.1

Williams, H., and Hiscott, R. N., 1987, Definition of the lapetus rift-drift transition in western Newfoundland: Geology, v. 15, n. 11, p. 1044–1047, https://doi.org/10.1130/0091-7613(1987)15<1044:DOTLRT>2.0.CO;2

Williams, H., and Stevens, R. K., 1974, The ancient continental margin of eastern North America, *in* Burk, C. A., and Drake, C. L. editors, The Geology of Continental Margins: New York, Springer-Verlag, p. 781–796, https://doi.org/10.1007/978-3-662-01141-6_58

Zagorevski, A., Lissenberg, C. J., and van Staal, C. R., 2009, Dynamics of accretion of arc and backarc crust to continental margins: Inferences from the Annieopsquotch accretionary tract, Newfoundland Appalachians: Tectonophysics, v. 479, n. 1–2, p. 150–164, https://doi.org/10.1016/j.tecto.2008.12.002